CITE AS: Liu Y, Malaga-Chuquitaype C, Elghazouli AY, 2012, Behaviour of beam-to-tubular column angle connections under shear loads, ENGINEERING STRUCTURES, Vol: 42, Pages: 434-456, ISSN: 0141-0296

Behaviour of beam-to-tubular column angle connections under shear loads

Y. Liu, C. Málaga-Chuquitaype, A. Y. Elghazouli[1]

Department of Civil and Environmental Engineering, Imperial College London, UK

ABSTRACT

This paper deals with the behaviour of semi-rigid angle connections between open beams and tubular columns under shear loads. It provides an account of six connection tests on blind-bolted as well as combined channel/angle configurations carried out under predominant shear loading conditions. The experimental set-up and specimen details are first introduced followed by a description of the results and experimental observations. A number of complementary simple and double shear tests on Hollo-bolt units are also reported in the paper. Based on the experimental results, the main behavioural patterns are discussed and the salient response characteristics related to stiffness and capacity are examined. Finite element models for simulating the joint behaviour are then proposed and a detailed description of the modelling assumptions is presented. Additionally, the potential applicability of simplified component-based expressions for the estimation of stiffness and capacity of beam-to-tubular column semi-rigid connections under shear loads is discussed. The experimental and numerical findings presented in this paper offer direct information on the influence of key geometric properties such as angle dimensions and column wall thickness on the main response characteristics. The results also provide essential data for future analytical and design-oriented studies.

Keywords: Semi-rigid joints, blind-bolted angle connections, combined channel/angle connections, tubular columns, shear loads.

1. Introduction

Hollow structural sections (HSS) exhibit inherent architectural and structural advantages over their open section counterparts. In particular, their relatively high strength to weight ratio and favourable torsional stiffness make HSS an ideal choice as column members. However, the difficulties associated with connection detailing, in particular with regards to connections between open beams and tubular columns may sometimes hamper their wider application in practice. Most of the research on open-

[1] Corresponding Author: Professor Ahmed Y. Elghazouli,
email:a.elghazouli@imperial.ac.uk,
Tel: +44 (0) 20 7594 6021, Fax: +44 (0) 20 7594 5934,

beam-to-tubular-column connections has focused on fully-rigid fully-welded details [1-4] and current European standards [5] incorporate rules for determining their resistance. In contrast, codified design guidance on semi-rigid/partial-strength bolted connections for tubes is lacking.

The cost and maintenance implications associated with welding have prompted the development of semi-rigid open beam-to-tubular column connection alternatives such as the flowdrill process [6-7] and special bolts with sleeves designed to expand inside the tube [8-9]. A simpler blind-bolt design is the Hollo-bolt, proposed by Lindapter International [10]. In particular, the wide availability and ease of use of the Hollo-bolt have motivated a number of experimental research studies on Hollo-bolted connections subjected mainly to bending and direct tension [6, 11-13]. France [6] carried out monotonic tests on three *end-plate* joints and compared the behaviour of blind-bolt and flowdrill forms. Adequate performance was reported with conventional drilling techniques being recommended for plates thicker than 12.5 mm. Nevertheless, issues of practicality make the application of flowdrilling relatively cumbersome and hinder its wider use. Barnet et al. [11-12] performed a review of different blind-bolting alternatives and carried out an experimental study on blind-bolted T-stubs and connections using Hollo-bolts. To improve the clamping mechanism, a modified blind-bolt, referred to as the Reverse Mechanism Hollo-Bolt (RMHB) was proposed. More recently, Elghazouli et al. [13] performed an experimental investigation into the monotonic and cyclic behaviour of *top and seat* and *top, seat and web angle* connections blind-bolted to structural hollow columns by means of Lindapter Hollo-bolts. It was shown that the grade of the Hollo-bolt, coupled with the gauge distance between the Hollo-bolt and beam flange, have a most notable effect on the flexural response of this type of connection. Nevertheless, information on the behaviour of blind-bolted connections under other loading conditions is still limited, particularly for angle connections subjected to shear loads. To this end, Yeomans [14] performed shear and tension tests to determine the capacity of Hollo-bolts and reported the failure shear load as a function of column thickness for Grade 8.8 M16 and M20 Hollo-bolts. However, a comprehensive characterization of the full shear force-displacement relationship of the Hollo-bolt insert and its underlying mechanisms has not been performed.

Whilst many studies have been carried out on the analytical modelling of semi-rigid connections incorporating conventional bolts [15-17], similar studies on blind-bolted connections to tubular columns are scarce. Ghobarah et al. [18] suggested a model for the estimation of the initial rotational stiffness and capacity of blind-bolted end-plate connections between open beams and tubular columns employing High Strength Blind-bolts [7, 9]. Wang et al. [19] investigated the moment-rotation behaviour of Hollo-bolted T-stubs and proposed an analytical model for the evaluation of their initial stiffness. Málaga-Chuquitaype and Elghazouli [20] proposed and validated a component-based mechanical model for blind-bolted angle connections able to trace the full monotonic and cyclic moment-rotation response of *top and seat* as well as *top,*

seat and web angle blind-bolted connections. Nevertheless, there is a need to characterize and incorporate the behaviour of blind-bolted angle connections subjected to shear into numerical and analytical tools.

Another alternative for bolted connections between open beams and tubular columns with the potential for wider application in practice is that offered by combined channel/angle configurations. This type of connection incorporates a channel section, which is shop-welded at the legs to the face of the column hence allowing the use of any conventional bolted detail between the reverse channel and open beams. Despite its versatility, there is a dearth of experimental studies on reverse channel configurations. Ding and Wang [21] compared the fire resistance of four end-plate reverse channel connections with other open beam-to-filled tubular column connection details. This study concluded that reverse channel connections can offer the best structural behaviour and cost-effectiveness among the different details considered. Málaga-Chuquitaype and Elghazouli [22] carried out an experimental study into the flexural behaviour of combined channel/angle connections under monotonic and cyclic loading. *Top and seat* as well as *top, seat and web angle* details were considered. It was observed that the flexibility of the reverse channel component has a direct influence on both the initial rotational stiffness and moment capacity of the connection, and the three main inelastic mechanisms exhibited by this type of connection were identified. It was also shown that simplified procedures adapted from the T-stub approach employed in Eurocode 3 [5], in conjunction with the use of appropriate gauge distances, can provide a conservative estimation of the connection moment capacity. However, as with blind-bolted details, there is a lack of experimental and numerical studies on the performance of combined channel/angle connections under other severe loading conditions such as shear actions.

This paper examines the shear behaviour of semi-rigid angle connections between open beams and tubular columns. It describes and discusses the results of three shear tests on Hollo-bolted angle connections and three tests on combined channel/angle connections. The experimental set-up, connection configurations and material properties are first introduced followed by an overview of the results and observations from the tests. Additionally, key results from complementary *simple and double shear* tests on Hollo-bolts are reported. Based on the experimental results, the main behavioural patterns are discussed and the salient response characteristics such as stiffness, capacity and failure mechanisms are examined. Furthermore, finite element models are developed and validated. It is demonstrated that these models can provide a realistic representation of the response of semi-rigid angle connections subjected to shear actions. Finally, the applicability of component-based approach for the estimation of connection stiffness and capacity is discussed.

2. Characteristics of Hollo-bolts in shear

2.1 General

Owing to its wide availability and ease of installation, the Hollo-bolt developed by Lindapter [10] was employed in this study to connect the angles to the column face in blind-bolted specimens. The response of Grade 8.8 Hollo-bolts subjected to direct tension and direct shear has been examined in previous studies [14, 23]. Yeomans [14] performed shear tests on grade 8.8 M16 and M20 Hollo-bolts connected to SHS columns. It was recommended that the Hollo-bolt shear capacity should be estimated on the basis of the shear resistance of the standard bolt with due account for the sleeve contribution. More recently Elghazouli et al. [13] reported axial force-displacement relationships for M16 and M12 Hollo-bolts with Grade 8.8 and 10.9 bolt shank subjected to pure tension. It was concluded that the higher torque permitted by Grade 10.9 bolts results in significant improvements in their axial stiffness in comparison with the corresponding Grade 8.8 bolts. However, a full characterization of the shear force-deformation relationships of Hollo-bolts is lacking. Therefore, and due to the direct relevance that the shear behaviour of the bolts is expected to have on the overall joint shear response, a number of *simple and double shear* tests on Hollow-bolt units were carried out as part of the present study. Normal bolts of the same diameter were also tested for comparison. The testing arrangement and specimen details are described below.

3.2 Direct shear tests

Figure 1 presents the arrangements used to perform the simple and double shear Hollo-bolt and standard bolt tests while Table 1 summarizes the test series. The specimen reference is expressed as M-d_1-d_2-F, where M stands for the configuration type (S for simple shear tests and D for double shear tests), F stands for the bolt type (where N represents the standard bolt and H represents the Hollo-bolt), and d_1 and d_2 are the connecting plate thicknesses as presented in Figure 1 and Table 1. In the case of double shear tests, two plates of the same thickness were used for the outer plates at each side. An actuator operating in displacement control was used to apply vertical displacements at the top of the connecting plates whilst the bottom end displacements were restrained. Vertical displacements and the corresponding forces were recorded by the load cell and transducer incorporated within the actuator. Both simple shear tests and double shear tests with varying plate thicknesses were conducted on Grade 10.9 M16 Hollo-bolts. These tests were complemented with simple shear tests on standard bolts for comparison purposes as summarized in Table 1.

Figure 2 depicts the observed deformation patterns for shear tests on Hollo-bolts while Figures 3 and 5 show the corresponding Hollo-bolt shear force-displacements obtained by means of the load cell and displacement transducer incorporated within the actuator. As expected, the plate thickness has a direct influence on the behaviour of the connection in shear and the associated deformation patterns. The plate

verticality was maintained up to displacements of around 3 mm in all specimens. In the case of simple shear connections, significant rotations start to accumulate for vertical displacements greater than 3mm. As shown in Figures 2(a) and 2(b), large rotations were observed at the end of the test in Specimens S-10-8-H and S-15-15-H coupled with plate local bearing deformations.

For Hollo-bolted simple shear specimens (S-10-8-H and S-15-15-H), Hollo-bolt sleeve yielding was observed at about 20 kN, followed by slippage. The ultimate response of Specimen S-10-8-H was dominated by the bearing capacity of the 8 mm plate whereas the thicker plates used in Specimen S-15-15-H caused the behaviour to be mainly determined by the Hollo-bolt response in shear, which reached failure at a load of about 159 kN corresponding to a displacement of approximately 13 mm.

In the case of Hollo-bolted double shear specimens (Specimens D-8-10-H and D-8-15-H) the Hollo-bolt sleeve yielded at about 40 kN. Importantly, due to unavoidable manufacturing differences, slippage was observed to happen at a load of around 15 kN in Specimen D-8-10-H while slippage occurred at a higher load of about 50 kN (after sleeve yielding) in the case of specimen D-8-15-H. On the other hand, large bearing deformations were evident in the middle plate at displacements of around 9.5 mm for both specimens. Besides, the ultimate load of Specimen D-8-15-H was about 50 kN higher than that of Specimen D-8-10-H as shown in Figure 3. This is attributed to the increase in bearing capacity of the connection due to the thicker middle plate.

In order to compare the shear resistance of Hollo-bolts against their standard bolt counterparts, simple shear tests were carried out on standard bolted specimens (S-10-8-N and S-15-15-N) as shown in Figures 4 and 5. It is evident from Figure 4 that the out-of-plane deformation of the connecting plates was notably lower than that observed in Hollo-bolted specimens (e.g. by comparing Specimens S-10-8-N and S-15-15-N in Figure 4 with Specimens S-10-8-H and S-15-15-H in Figure 2). This increased out-of-plane deformation in blind-bolted connections is attributed to the larger bolt hole diameter that is necessary to accommodate the Hollo-bolt insert which causes a reduction in the corresponding plate stiffness. Specimen S-10-8-N as well as S-15-15-N failed due to shear fracture of the bolt at loads of 109 kN and 116 kN corresponding to displacements of 9 mm and 6 mm, respectively.

Figure 5 compares the shear force-displacement relationships between standard and Hollo-bolts subjected to simple shear action as described above. Ultimate bolt shear and plate bearing capacity estimates are also included in Figure 5 for comparison. The shear capacity of standard bolts per shear plane, V_s, was estimated through the following relationship:

$$V_s = \frac{A_v f_u}{\sqrt{3}} \qquad (1)$$

where, A_v is the stress area of the bolt shank and f_u its ultimate strength. Similarly, the shear capacity of Hollo-bolts was calculated as:

$$V_H = \frac{A_v f_u + A_{vs} f_{us}}{\sqrt{3}} \qquad (2)$$

where, A_{vs} and f_{us} are the sleeve area and ultimate strength, respectively. A value of 509 N/mm2 was used for the sleeve strength as obtained from the mean of three hardness tests. The consideration of the shear resistance contribution of the Hollo-bolt sleeve in Equation 2 resulted in a 20 kN increase in the nominal shear capacity of M16 Hollo-bolts with respect to the corresponding standard bolt. Likewise, based on strength values obtained from coupon tests reported in Table 2, the plate bearing design capacities were calculated as 120 kN and 230 kN for 8 mm (from Angle L100×75×8) and 15 mm (from Angle L150×80×15) steel plates, respectively.

It can be observed from Figure 5 that in the case of Hollo-bolted specimens, the initial stiffness is maintained up to a shear force of about 20 kN, when yielding of the sleeve occurs, followed by considerable post-yield hardening. After yielding of the Hollo-bolt sleeve, contact between the sleeve and the shank takes place and the applied shear force is gradually transmitted to the bolt shank up to the occurrence of plate bearing failure (at 124 kN for Specimen S-10-8-H in Figure 5(a)) or shear fracture of the shank (at 165 kN for Specimen S-15-15-H in Figure 5(b)). Conversely, the standard bolt specimens experienced bolt slippage between 0.5 mm and 2 mm of relative displacement. Importantly, bolt shear fracture occurred at a shear load of 115 kN in standard bolts (Specimen S-10-8-N and S-15-15-N) which is 18% higher than the shear capacity estimate obtained by means of Equation 1. On the other hand, shear fracture of the bolt shank in Hollo-bolts are delayed up to a load of about 160kN in the case of Specimen S-15-15-H which is 28% higher than the estimate of Equation 2. This can be attributed in part to the significant rotation observed in Specimen S-15-15-H leading to the change in the orientation of the effective shear plane and thus reduced shear loading component coupled with possible variations in the nominal versus actual ultimate bolt strength. In general, it can be concluded that Equations 1 and 2 offer conservative estimates of ultimate bolt shear capacities. Moreover, it can also be observed from Figure 5 that blind-bolted connections subjected to shear are able to provide up to twice the ductility capacity of standard bolted connections owing to the presence of the flexible sleeve that delays the fracture of the bolt until considerably larger deformation levels.

The behaviour of Hollo-bolts in shear has a direct influence on the response of angle connections, as discussed in subsequent sections.

3. Testing arrangement and connection details

3.1 Experimental set-up

The set-up used for testing the beam-to-tubular column connections in shear is shown in Figure 6. A column section of 800 mm height was used in all tests. The column was fixed at both ends by welding it to a 10 mm plate clamped at the base and bolting it to a lateral bracing at the top, as depicted in Figure 6(a). A hydraulic actuator operating in displacement control was used to apply vertical deformations at the head of the bolts connecting the beam and top angle. The force imposed by the actuator was transmitted through a heavy-section I-beam and a bearing plate of 30 mm thickness in order to achieve an even distribution of stresses over the head of the top angle bolts, as shown in Figure 6(b). In the case of the web angle connections, a 30 mm plate was placed on the top beam flange in line with the bolts connecting the beam web side of the web angles. The displacement at the head of the top angle bolts (for top and seat angle connections) and at the top beam flange (in the case of web angle connections) was gradually increased up to a maximum vertical displacement of 16 mm, or until the capacity of the actuator was reached (at around 600 kN).

The applied vertical displacement and corresponding vertical force were recorded by the load cell and transducer incorporated within the actuator. The verticality of the column was monitored through a displacement transducer placed at the top of the column, while a series of other independently referenced transducers measured displacements at a number of locations within the beam. Strain gauges were used to monitor the strains at expected inelastic regions within the angles.

3.2 Connection specimens

Six open beam-to-tubular column angle connections were examined: three Hollo-bolted and three reverse channel details. A summary of the test series is given in Table 3, including the geometric details of the connection as well as the column and reverse channel sizes. In the table, SHS refers to Square Hollow Section columns and L refers to angle. Figure 7 depicts the connection configurations studied (Type A used in Hollo-bolted specimens and Types B and C utilized in reverse channel configurations). The reference employed for the specimens is expressed by *Pt-Nx-Gy-T* for top and seat angle specimens whereas *Pt-Nx-Gy-W* was used for specimens incorporating web angle components. In this nomenclature, *P* represents the connection type (*H* stands for the blind-bolted angle connection and *R* stands for combined channel/angle connection), *t* is the thickness of the column or channel in mm, *x* is the thickness of the angle in mm, and *y* expresses the gauge distance between the centre of the bolt hole in the horizontal angle leg and column flange in mm (i.e. the value of *a* as indicated in Figure 7). Universal beams UB 305×102×25 and Grade 10.9 M16 standard bolts were employed in all cases. The grade of the steel used for beams, columns and angles was S275. Table 2 presents the mean yield stress values

and ultimate strength for the angle, beam and column components as obtained from at least three coupon tests in each case.

Preliminary numerical studies carried out as part of the present research [24] have shown that the beam web stiffness has a vital role on the shear performance of the connection. Buckling of the beam web can prevent the connection from reaching its maximum shear capacity and initiate complicated local effects. Therefore, in order to focus on the shear behaviour of the connection, web stiffeners were used to prevent premature local buckling effects, as shown in Figure 7. This enabled a better understanding of the basic behavioural mechanisms of bolt, angle and column face components under shear loading. To this end, the beam web was stiffened in *top and seat* angle connections (Figures 7(a) and 7(b)) by means of four 10 mm steel plates (two at each side) welded perpendicular to the web along the full beam depth. Similarly, in the case of reverse channel connections with web angles (Specimen R10-N8-G50-W), the beam web was stiffened by welding 10 mm-thick plates on each side inbetween the web angles and the beam web as depicted in Figure 7(c).

Grade 10.9 M16 Hollo-bolts were used for the blind-bolted configurations. Tightening torques of 315 and 244 Nm were applied to the standard and Hollo-bolts, respectively, by means of calibrated external torque devices; these torque levels are assumed to produce preloads of 110 and 85 kN for standard and Hollo-bolts, respectively, based on manufacturer information. Also, the reverse channel components used for combined channel/angle connections were obtained from SHS by longitudinal cutting, as performed in previous studies on this type of connections [22]. Table 3 gives the dimensions of the SHS from which the reverse channels were obtained. Fillet welding with 10 mm thickness was used to connect the column and the reverse channel throughout the length of the channel component.

4. Results and observations from connection tests

Table 4 summarises the main response parameters obtained from the shear tests on blind-bolted and reverse channel connections, while Figures 8-16 present the key results in terms of deformation patterns and shear force-displacement relationships obtained by means of the load cell and displacement transducer incorporated within the actuator. The initial stiffness and yield force presented in Table 4 were obtained from a bilinear idealization of the corresponding shear force-displacement curves. The observed shear forces at an applied displacement of 8 mm are also reported in Table 4 for comparative purposes. In subsequent sections, the experimental results and observations from the three blind-bolted as well as the three combined channel/angle connection specimens are presented and discussed with particular focus on the influence of the following key parameters on the connection behaviour: (i) gauge distance, (ii) angle thickness, (iii) channel thickness and (iv) presence of web angles.

4.1 Blind-bolted angle connections

4.1.1 Deformation patterns

Figure 8 presents the deformation patterns identified for the blind-bolted connection specimens at a displacement of 16 mm. As expected, the deformation patterns observed in Hollo-bolted connections subjected to shear result from the behaviour of individual components and their interactions. It can be observed from Figure 8(a) that plasticity occurred at the toe of the vertical leg of the top angle in Specimen H10-N8-G45-T, while large plastic deformations were concentrated in the horizontal leg of the top angle in Specimen H10-N8-G50-T (Figure 8(b)). On the other hand, significant bearing deformation in the bottom angle vertical (column) leg was evident in both Specimens H10-N8-G45-T and H10-N8-G50-T with some observed rotation taking place in the bottom angle in Specimen H10-N8-G50-T. These small rotations observed in Specimen H10-N8-G50-T are attributed to the increased horizontal gauge distance *a* that generates larger flexural action. In contrast, when the thickness of the angle is increased to 15 mm (i.e. Specimen H10-N15-G50-T in Figure 8 (c)), the plastic deformation tended to concentrate in bearing within the column face. It can also be observed from Figure 8(c), that limited deformations occurred in the bottom angle when a thick angle (15 mm) was employed.

The shear force-displacement relationships for the Hollo-bolted connections are depicted in Figure 9, whilst Figure 10 illustrates the development of plasticity in the top and bottom angles through measured strain values at selected locations. These figures are discussed in more detail in subsequent sections with focus on the influence of specific geometric parameters, namely the gauge distance and angle thickness, on the connection response.

4.1.2 Geometric parameters

The influence of the connection geometric parameters and their interrelation can be examined by comparing the results of Specimen H10-N8-G45-T (with a = 45 mm and d = 65 mm) and Specimen H10-N8-G50-T (with a = 50 mm and d = 40 mm). The shear-displacement responses of specimens H10-N8-G45-T and H10-N8-G50-T are presented in Figure 9 and the key response parameters are summarized in Table 4. It can be seen from Table 4 and Figure 9, that the initial stiffness of Specimen H10-N8-G45-T was about 14% larger than that of Specimen H10-N8-G50-T. This difference can be largely attributed to the stiffer horizontal angle leg and the relatively minor influence of the vertical leg of the angle during the initial stages of shear deformation. The stiffer response of Specimen H10-N8-G45-T is maintained until the attainment of the connection shear yield capacity when Specimen H10-N8-G45-T developed a yield force 19% higher than Specimen H10-N8-G50-T. Nevertheless, similar shear force-displacement responses can be observed for both specimens after yielding due to the accumulation of deformations in the vertical leg of Specimen H10-N8-G45-T.

The location and extent of plasticity in the angles in Specimens H10-N8-G45-T and H10-N8-G50-T can be further examined with reference to the strain measurements depicted in Figures 10(b) and (c). As shown in Figure 10(b), for Specimen H10-N8-G45-T, yielding strains were first reached near the toe of the vertical angle leg (location S2 in Figure 10(a)) followed by the development of large plastic deformations. Plastic strain levels were also attained in the horizontal leg between the bolts for joint vertical displacements over 3 mm. With regards to Specimen H10-N8-G50-T shown in Figure 10(c), more significant plastic deformations were induced in the horizontal angle leg (locations S3 and S4 in Figure 10(a)) with the vertical angle leg remaining elastic up to a vertical displacement of around 8 mm. These results highlight the interrelation between the vertical and horizontal gauge distances in the top angle for different deformation stages. For lower deformation levels, the initial response of the top angle is mainly determined by its horizontal gauge distance (a in Figure 7). However, after plasticity is attained and as the joint shear deformations increase, the flexibility of the vertical angel leg started gaining importance. It is also worth noting that the deformation modes of the bottom angles in Specimens H10-N8-G45-T and H10-N8-G50-T were different as observed from Figures 8 (a), 8 (b), 10 (b) and 10(c). For Specimen H10-N8-G45-T, the main plastic deformations were concentrated in the vertical leg, while the horizontal leg (Location S8 in Figure 10(a)) remained elastic. In contrast, plasticity occurred in the horizontal leg (location S5 in Figure 10(a)) for Specimen H10-N8-G50-T with the vertical leg remaining elastic. This can be attributed to the larger horizontal gauge distance leading to increased rotation of the beam which in turn also caused a change in the deformation pattern of the bottom angle from bearing in Specimen H10-N8-G45-T to bending in Specimen H10-N8-G50-T.

4.1.3 Angle thickness

The influence of angle thickness can be illustrated by comparing the results of specimens H10-N8-G50-T and H10-N15-G50-T where the angle was varied from L100×75×8 in the former to L150×80×15 in the latter. As expected, the thickness of the angle has a direct effect on the connection response, including the stiffness, capacity, and deformation modes. As indicated in Figure 9 and Table 4, the initial stiffness of Specimen H10-N15-G50-T which incorporates a thicker angle was around 55% larger than that of Specimen H10-N8-G50-T, while the capacity at an applied displacement of 8 mm for the former was also 100 kN higher than the latter, respectively. The differences in deformation modes for top and bottom angles between Specimens H10-N8-G50-T and H10-N15-G50-T become evident by comparing Figures 8(b) and 8(c). These differences can be better understood with reference to the development of the strains shown in Figures 10(c) and (d). In the case of Specimen H10-N15-G50-T, plastic deformations in the top angle first occurred in the horizontal leg between the bolts (Location S4 in Figure 10(a)), while at other strain gauge locations, plastic strain was not reached until a displacement of 8 mm. Moreover, only limited plastic deformation developed in the bottom angle as shown

in Figure 10(d), whereas significant plastic deformation accumulated in both top and seat angles in the case of Specimen H10-N8-G50-T as described previously.

4.2 Combined channel/angle connections

4.2.1 Deformation patterns

The main deformation patterns of the three combined channel/angle connection specimens tested are depicted in Figure 11. In the case of Specimen R10-N8-G45-T, shown in Figure 11(a), the bending deformation of the top angle and the bolt shear deformation in the bottom angle region dominated the overall joint shear behaviour. Significant plasticity occurred in the vertical leg of the top angle, whilst the bottom bolts failed in shear at a displacement of 11 mm. On the other hand, when thicker angles were combined with a thinner channel in the case of Specimen R6.3-N15-G50-T (Figure 11(b)), the failure mechanism was determined by the top region of the channel flange under combined shear and axial load. This axial load originated from the slight rotation of the beam caused by the offset distance between the loading point and channel face, hence the vertical leg of the top angle moved outwards together with the vertical deformation. Large bearing deformation also occurred in the bottom channel flange with simultaneous bolt shear deformation. Specimen R6.3-N15-G50-T also failed by shear fracture of the bolts connecting the bottom angle and the channel components at a displacement of around 11 mm. Finally, two main deformation components were identifiable in the response of the double web angle connection (Specimen R10-N8-G50-W presented in Figure 11(c)): web angle bearing and bolt shearing. Importantly, the test on Specimen R10-N8-G50-W reached the actuator load capacity (600 kN) at a displacement of nearly 9 mm without signs of failure. The shear force-displacement relationships for Specimens R10-N8-G45-T, R6.3-N15-G50-T and R10-N8-G50-W are depicted in Figure 12. These relationships, together with the above descriptions will be discussed further in subsequent sub-sections of this paper with emphasis on the influence of angle and channel thickness as well as web angle contribution.

4.2.2 Component stiffness

The effects of the thickness of angle and reverse channel components on the shear response of combined channel/angle connections can be explored by comparing the experimental results of Specimens R10-N8-G45-T and R6.3-N15-G50-T. It can be observed from Table 4 and Figure 12 that the stiffness of Specimen R10-N8-G45-T is 34% higher than that of Specimen R6.3-N15-G50-T. Although the thicker angle improved the stiffness of Specimen R6.3-N15-G50-T, the increased bearing flexibility of the thinner channel used in Specimen R6.3-N15-G50-T relative to Specimen R10-N8-G45-T, coupled with the larger horizontal gauge distance, led to an overall lower initial stiffness. In general, the shear force-displacement responses of Specimens R10-N8-G45-T and R6.3-N15-G50-T are similar despite the notable differences in their deformation modes, with the deformation of the reverse channel/bolt assemblage

dominating the response of Specimen R6.3-N15-G50-T. Importantly, bolt slip occurred almost instantaneously at a load level of 100 kN in Specimen R10-N8-G45-T whereas a more gradual slip was observed in Specimen R6.3-N15-G50-T. The above discussion can be confirmed with reference to the development of strains measured in Specimens R10-N8-G45-T and R6.3-N15-G50-T, and presented in Figures 13(b) and (c), respectively. It can be seen from Figure 13(b) that the yield strain was reached in the toe of the horizontal leg (Location S2 in Figure 13(a)) of the top angle of Specimen R10-N8-G45-T at an overall joint vertical displacement of nearly 2 mm. In contrast, the thicker top angle employed in Specimen R6.3-N15-G50-T remained elastic in almost all monitoring points except for the area in the horizontal leg around the bolts below the loading plate (Location S4 in Figure 13(a)). Moreover, Specimen R10-N8-G45-T developed significant plastic deformation due to bearing in the bottom angle leg (Location S6 in Figure 13(b)).

4.2.3 Web angles

The response of double web angle reverse channel connections under shear was examined through Specimen R10-N8-G45-T. As illustrated in Figure 12 and Table 4, the web angle configuration exhibited significantly higher stiffness and capacity when compared with top and seat angle details. In comparison with Specimen R10-N8-G45-T, for example, the initial stiffness and ultimate capacity of Specimen R10-N8-G50-W reached almost a threefold increase. Figure 14(b) depicts the measured strains in Specimen R10-N8-G50-W, in which it is observed that the bearing strain in the lateral leg around the top bolt of the left web angle (Location S1 in Figure 14(a)) was around twice as much as the corresponding strain near the bottom two locations (S2 and S3 in Figure 14(a)) at an applied displacement of around 8 mm. Conversely, on the leg of the parallel web angle, the strain levels near the bottom bolt (Location S6 in Figure 14(a)) were larger than at Locations S4 and S5 in Figure 14(a). This uneven distribution of stresses and strains is attributed to the unavoidable differences in bolt hole tolerances during manufacturing.

4. 3 Ductility considerations

The experimental results described above show that blind-bolted angle connections can provide significant levels of ductility in shear exceeding 16 mm of vertical displacement without notable deterioration in capacity (Figure 9). These high ductility levels are attributed to the Hollo-bolt insert contribution in shear as reported in Section 2.3. In contrast, the combined channel/angle connection specimens (R10-N8-G45-T and R6.3-N15-G50-T) failed by shear fracture of the standard bolts at around 11 mm of vertical displacement (Figure 12). Also, the stiffness and capacity of connections incorporating web angle/channel components (i.e. Specimen R8-N10-G50-W) can be significantly enhanced due to the increased shear stiffness of the web angle components and the larger number of bolts acting in shear.

5. Numerical assessment

Due to the large number of inter-related parameters that can influence the shear response of bolted open beam-to-tubular column connections, assessing their behaviour solely on the basis of experimental investigations is a cost-prohibitive and time-consuming task. Therefore, the use of appropriately validated finite element models represents an attractive approach for the future development of a database of connection characteristics. Such numerical simulations can also offer valuable insight into the intricate component interactions that occur within semi-rigid open beam-to-tubular column connections. To this end, three-dimensional finite element (FE) models are constructed herein by means of the commercial FE software ABAQUS [25], and the results are validated against the experimental data described above. Particular emphasis is given in the discussion presented below to aspects related to key design parameters such as initial stiffness, ultimate load and failure mode.

5.1 Finite element modelling

The different connection components were modelled by means of eight-node brick solid elements of Type C3D8I available in the ABAQUS library [25], as shown in Figure 15. Special attention was paid to faithful modelling of the geometric details of the bolts including the shank, sleeve, head and nut, as depicted in Figure 16. The boundary conditions and loading procedure adopted in the numerical analyses replicated those used in the experimental studies described in previous sections. A number of mesh sensitivity studies were carried out in order to arrive at an optimum representation which involves a comparatively finer mesh for the angles and bolts, as well as the areas within the beams and columns in contact with these components, whereas a relatively coarser mesh was employed elsewhere. The dimensions of elements within the final adopted mesh ranged between 6 mm within the refined region, and up to 100 mm within the coarser region. The numerical models incorporated a number of detailed features such as loading reversal, contact phenomena, bolt slippage definition and bolt pretension application, as described below.

5.1.1 Contact surfaces

The contact phenomenon between two surfaces was taken into account by defining ‘hard and friction’ surface interaction. Contact was defined between the beam-to-column, top angle-to-beam, top angle-to-column, bottom angle-to-beam, bottom angle-to-column, and bolt-to-hole surfaces. The more flexible surface was chosen as slave, while that on the stiffer component was designated as master. Moreover, the slippage between the bolt and hole surfaces was considered by defining a contact interaction with an assumed friction coefficient of 0.25 for all cases.

5.1.2 Bolt pre-tension

Bolt pretension in standard and Hollo-bolts was introduced by means of two loading steps. Firstly, pretension forces for Grade 10.9 M16 bolts were applied, in accordance with the specified tightening torques. The second step involved removing the applied pretension force while simultaneously fixing the bolt length at its deformed (shortened) value.

5.1.3 Hollo-bolt representation

Figure 16 shows a view of the clamping mechanism of the Lindapter Hollo-bolt used in this study as well as its FE model representation. The proposed FE model simulates the central bolt, sleeve body and cone by separate individual components. The Hollo-bolt sleeve model was constructed with due account of the actual geometrical characteristics of the Hollo-bolt. The contact properties between shank surface and sleeve surface as well as cone and sleeve surface were defined as 'hard and friction contact' following the procedure described above. The cone was tied to the bolt shank, and the corresponding pretension loads were directly applied to the shank.

5.2 Simulation of tests

The FE model described above was used to simulate the tests from the experimental programme presented in Section 3. Numerical shear force-displacement relationships are compared with their corresponding experimental curves in Figures 17 to 21. The FE validation and modelling implications are discussed below for standard and Hollo-bolts, blind-bolted connections and combined channel/angle connections.

5.2.1 Direct shear response

The experimental shear force-displacement relationships for simple and double shear tests on standard and Hollo-bolts are presented in Figure 17 together with their corresponding FE predictions. It is evident from Figure 17 that the FE models provide a reasonably accurate representation of the experimental behaviour in all cases. In particular, the initial stiffness, yield point and post-yield response closely match the experimental values.

Specimen S-10-8-H is taken herein as a typical example for a more detailed discussion. The shear force-displacement relationships, obtained from experimental results as well as FE simulation, and Von Misses Stress distribution of the joint at four significant points are depicted in Figure 18. It is shown in the figure that the main behavioural characteristics observed during the experiment are well represented by the FE analysis. The FE model in turn, enables the identification of the key deformation stages in the shear force-displacement response of Specimen S-10-8-H. To this end, the first significant point, identified as B1 in Figure 18, occurs at a shear load of nearly 20 kN corresponding to yielding of the Hollo-bolt sleeve. This stage is evident in both the numerical and experimental curves and is further confirmed by the maximum stress levels obtained from cross-sectional views of the Hollo-bolt which

are also presented in Figure 18. After yielding of the Hollo-bolt sleeve, significant localized deformations are developed which eventually lead to full contact between the sleeve and bolt shank at point B2 in Figure 18. At a shear load of about 80 kN (point B3), yielding of the 8 mm plate in bearing takes place followed by large plastic bearing deformations (up to point B4). It can be concluded from the above discussion and results that the proposed FE model is able to simulate reasonably well the evolution of shear forces and local deformations on the standard and/or Hollo-bolt/plate assemblage.

5.2.2 Blind-bolted angle connections

Figure 19 compares the shear force-displacement relationships of the blind-bolted connection tests (i.e. Specimens H10-N8-G45-T, H10-N8-G50-T and H10-N15-G50-T). It can be noted from Figure 19 that reasonable estimates of stiffness and capacity are obtained in all cases. The differences between the experimental results and numerical simulations observed (in the range from 0.2 mm to 1.2 mm of vertical displacement) can be attributed to bolt slippage. Importantly, in the FE simulation, slippage of the bolt occurs almost instantaneously once the friction forces are overcome, whereas a more gradual slip displacement is observed during the test. Similarly, good agreement can be observed between the capacity estimations of the FE model and the experimental values within a difference of ±10%. The relatively minor discrepancies at large displacements observed in Figure 19 are attributed to unavoidable differences between the material strain hardening material characteristics assumed for the FE models and those of the different components used in the tests. Also, it is worth noting that in the case of Specimen H10-N15-G50-T (Figure 19(c)), an abrupt transition between flexure-dominated and bearing-dominated plastic mechanisms occurred at a vertical displacement of around 11.5 mm in the numerical simulation whereas a more gradual change was observed during the experiment. This can be attributed to the small difference in the clamping angle of the deformed sleeve after installation, leading to pull-out of the Hollo-bolt in the FE model at around 11.5 mm of joint shear displacement. This causes noticeable reduction in force and re-arrangement of the Hollo-bolt component deformations after which the loading force starts to increase, all of which occurred in a more gradual manner during the test.

Figure 20 illustrates the deformation pattern observed in the top angle of Specimens H10-N8-G45-T, H10-N8-G50-T and H10-N15-G50-T at a vertical displacement of 16 mm and compares it with the FE model prediction. It is evident from Figure 20 that the deformation and plastic mechanism are replicated by the proposed FE models. To support this, the measured strains at Location S2 and S3 (indicated in Figure 10(a)) of the top angle in Hollo-bolted specimens are compared against their corresponding numerical predictions in Figure 21. From the figure, a good correlation between the experimentally observed and numerically estimated strain values can be noted both in the pre-yielding range and up to large levels of displacement demand. This agreement shows that the detailed FE model can faithfully simulate the shear response of blind-bolted angle connections.

5.2.3 Combined channel/angle connections

Contrary to blind-bolted connections, in which contact between the blind-bolt sleeve and the connecting angle/column plates is present from the onset, the use of standard bolts in reverse channel configurations involves the provision of bolt hole tolerances that can play an important role in the overall joint response under shear loads. To this end, a series of sensitivity analyses were performed in order to investigate the influence of possible tolerance variation as well as the assumed friction coefficient on the stiffness and capacity of combined channel/angle connections [24]. It was concluded that an average friction coefficient of 0.25 coupled with hole tolerances in the range of 2 mm leads to a better representation of the experimental results.

Figure 22 presents the numerical shear force-displacement relationships for Specimens R10-N8-G45-T, R6.3-N15-G50-T and R10-N8-G50-W together with the corresponding experimental curves. It is observed from Figure 22 that the initial stiffness and connection capacity are well estimated by the FE representation. The discrepancies in post-yield stiffness observed in Figure 22 are related to differences in the evolution of bolt slippage displacement between the FE models and the experimental results. Notably, in the case of Specimen R6.3-N15-G50-T (Figure 22(b)), instantaneous slippage occurred at a load level of nearly 100 kN in the FE model whereas a gradual and sustained accumulation of slip deformations was noticeable in the experiment, starting at a load of around 70 kN. The same is true for Specimen R10-N8-G50-W where the multiple slip paths in the web angle components originated distinguishable short slip-only deformations at load levels of 100 and 180 kN approximately, while a more gradual accumulation of deformation was observed during the test.

Finally, Figure 23 compares the experimentally observed plastic deformations in combined channel angle specimens against their numerical predictions. It is evident from this figure that the proposed FE models are able to accurately replicate the observed plastic deformation modes. Similarly, Figure 24 presents the comparison in terms of strains at Locations S2 and S3 (indicated in Figure 13) for Specimens R10-N8-G45-T and R6.3-N15-G50-T and at Locations S1 and S6 (indicated in Figure 14) for Specimen R10-N8-G50-W. A reasonably good correlation is apparent from these figures which show that the detailed FE model can faithfully simulate the shear response of reverse channel connections.

6. Parameter estimation

In some situations, such as those involving extreme accidental scenarios, considerable shear actions can be induced in the joints and the survivability of the structure may largely rely on the connection ability to sustain significant forces or deformations under predominant shear actions [26]. Also, it can be demonstrated [24] that when loads are applied near the connection, significant deformations can accumulate and the shear stiffness of the connection should be taken into consideration. To this end,

the experimental results and numerical models presented in previous sections provide essential data and information for undertaking detailed design-oriented studies for connections under such circumstances. Extensive parametric analyses are currently underway, with a view to developing design methodologies for the consideration of shear action in open beam-to-tubular column bolted connections. Nevertheless, in light of the findings described above, it is useful at this stage to offer a preliminary assessment of available design expressions for the evaluation of connection stiffness as well as yield and failure capacities. To this end, the well established component-based approach [5] is considered herein together with available component characterizations [27].

6.1 Connection stiffness

The initial shear stiffness of bolted connections to tubular columns can be evaluated from the contributions of the angle bending stiffness (K_{tab}), angle leg bearing stiffness (K_{ab}), bearing stiffness of the column/channel face (K_{cb}), the Hollo-bolt or axial bolt shear stiffness (K_{bs}) as well as the effective rotational stiffness of the top angle (K_r). Therefore, the initial stiffness of top and seat angle connections can be defined as:

$$K = K_{top} + K_{bottom} = \frac{1}{\frac{1}{K_r} + \frac{1}{K_{tab}} + \frac{1}{K_{ab}} + \frac{1}{K_{cb}} + \frac{1}{K_{bs}}} + \frac{1}{\frac{1}{K_{ab}} + \frac{1}{K_{cb}} + \frac{1}{K_{bs}}} \qquad (3)$$

where K_{tab}, K_{ab}, K_{cb} and K_{bs} can be obtained from the corresponding expressions proposed by Faella et al. [27] for equivalent T-stubs with due consideration of the loading direction and component orientation. Additionally, the top angle rotational stiffness (K_r) can be estimated as:

$$K_r = \frac{d^2}{a_2}\left(\frac{1}{\frac{1}{K_{ct}} + \frac{1}{K_{bt}}}\right) \qquad (4)$$

where K_{ct} is the column or channel face tension stiffness as defined by Málaga-Chuquitaye and Elghazouli [20], K_{bt} is the bolt stiffness in tension and the dimensions *a* and *d* are the nominal gauge distances depicted in Figure 7.

Similarly, when web angles are incorporated, the connection stiffness can be estimated from:

$$K = \sum_{i=1}^{n_r} K_i \qquad (5)$$

where n_r is the number of bolt rows, K_i is the stiffness of the ith bolt-row defined as:

$$K_i = \frac{2}{\frac{1}{K_{ab}} + \frac{2}{K_{bs}} + \frac{1}{K_{cb}}} \qquad (6)$$

Figures 24 and 25 present a comparison of the experimental curves with the stiffness estimations obtained by means of Equations 3 to 4. It can be observed from these figures that the equations presented above provide a good estimation, well within 10% accuracy, of the connection stiffness for all Specimens. It is important to note that in the case of Specimens H10-N15-G50-T and R6.3-N15-G50-T, which incorporate stiffer angles, the contribution of the top angle rotational deformation (Equation 4) accounted for 20-30% of the overall joint flexibility due to the relatively higher tensile forces transmitted onto the column/channel face in these specimens. Conversely, the effects of angle rotation in the other connection specimens were found to be relatively minor.

6.2 Yield and ultimate capacities

As noted in previous sections, the connection shear response involves complex interactions that cause yielding in a particular component followed by slip or yielding in alternative connection zones and can eventually lead to bolt fracture or bearing failure. These intricate phenomena are further complicated by slight variations in hole tolerances and uncertainties in the initial placement of bolts within the holes. Therefore, this section offers a preliminary assessment of yield and ultimate capacities of bolted angle connections to tubular columns. Available expressions [27] for the determination of specific component yield and ultimate resistances are employed.

6.2.1 Yield force

In the case of Hollo-bolted connections, the initial yield in shear can be marked by the occurrence of yield within the Hollo-bolt sleeve (at 16 kN for each M16 Hollo-bolt). Nevertheless, only relatively small deformation would occur thereafter and yielding of additional connection components would be expected before significant accumulation of displacement takes place. Accordingly, an upper bound estimate of the connection yield capacity can be obtained from the yielding of the second weakest component, plus any additional load contribution of the other connection bolt-rows.

Figure 24 presents the regions demarcated by the lower and upper bound estimates described above together with the experimental force-displacement curves. It appears from Figure 24 that the experimental yielding forces of Specimens H10-N8-G50-T (Figure 24(b)) and H10-N15-G50-T (Figure 24(c)) are bounded by the two yield estimates. On the other hand, the upper bound estimate of yield force (corresponding to top angle in bending plus the corresponding bottom angle force) depicts the observed yield force in Specimen H10-N8-G45-T of Figure 24(a). These variations can be attributed to differences in hole tolerances that can accentuate the blind-bolt rotation after sleeve yielding in some cases while preventing significant displacement accumulation in others.

In the case of reverse channel configurations, the estimates of yield force can be obtained from yielding of the weakest constituent plus any additional load contribution arising from other connection components. These yield force estimates are presented in Figure 25 together with slip resistance values (at about 25 kN per standard bolt). It is clear from Figure 25 that the suggested simplified procedure provides reasonable estimations of yield shear force in all cases. Also, bolt slippage seems to be largely concurrent with yielding in the case of Specimens R10-N8-G45-T and R6.3-N15-G50-T of Figures 25(a) and 25(b), respectively.

6.2.2 Ultimate capacity

A specific definition of failure criteria for bolted connections under shear loading is out of the scope of the present paper. However, an often conservative approach would be to define the ultimate load as that corresponding to the summation of capacities of the weakest components within each bolt-row. These ultimate capacity values are presented in Figures 24 and 25 and compared with the experimental curves for Hollo-bolted and reverse channel connections, respectively. It is apparent from these figures that the above mentioned scenario offers a conservative estimation of the experimentally obtained failure load of Specimens H10-N8-G45-T, H10-N8-G50-T, H10-N15-G50-T, R10-N8-G45-T and R10-N8-G50-W. However, the ultimate load is overestimated in the case of Specimen R6.3-N15-G50-T (Figure 25 (b)), which does not reach the ultimate capacity based on shear fracture of standard bolts (376 kN). This discrepancy can be attributed to additional tension stresses in the bolt caused by the rotation of the top angle observed in the test which may have been intensified by the prying action induced by the thin channel employed.

6.3 Practical application

The experimental and numerical results presented in this paper offer significant insight into the behaviour of blind-bolted and reverse channel connections under shear action. Although the test results indicate satisfactory inelastic performance and high levels of ductility, there are a number of practical design aspects that require further study. As noted previously, the stiffness of the connection is a key design parameter, and the component-based approach seems to provide reasonably good estimations. Similarly, available expressions for the evaluation of yield and ultimate capacities can provide a conservative estimate of these design parameters in most cases. Nevertheless, the consideration of aspects related to the difference of oversized Hollo-bolt holes and gauge distance on the plastic hinge formation in angles need to be examined further before such expressions can be used with confidence.

Another important design consideration is related to the ductility supply within the connections. In particular, the presence of the additional sleeve in the case of Hollo-bolt was observed to lead to up to a two-fold increase in the connection ductility which was also accompanied by an increased ultimate bolt shear capacity.

Finally, it is important to note that this work has focused on characterising the response of connections subjected to predominant shear actions. Nevertheless, the findings of this study can be applied to generalised loading conditions by combining the component characteristics in shear with those already available for other actions [13, 20, 22]. However, such generalizations will need to explicitly include the effects of prying action and possible load reversals.

7. Concluding remarks

The shear behaviour of bolted angle connections between tubular columns and open beams has been examined in this paper. An experimental programme comprising three shear tests on blind-bolted angle connections and three tests on combined channel/angle connections, as well as complementary tests on single and double lap joints, has been described. The main behavioural patterns were identified, and the key response characteristics such as stiffness, capacity and failure mechanism were discussed. The experimental results were also compared with detailed finite element simulations.

It was observed that the inelastic mechanisms exhibited by the connections studied herein under shear loads primarily involved the interaction between the angles and column/channel face components. As expected, it was shown that the angle horizontal gauge distance between the bolts and the column flange has a direct influence on the initial stiffness with a significant effect on the shear capacity of the connection. Importantly, the thickness of the angle has a direct influence on the initial stiffness and ultimate capacity of the connection. Similarly, the thickness of the reverse channel directly affects the connection stiffness and capacity. Besides, it was observed that the overall stiffness and resistance of the reverse channel connections with double web angels was enhanced significantly in comparison with those of the connections with top and seat angles only.

In terms of ductility, the blind-bolted angle connections provided significant deformation levels exceeding 16 mm of vertical displacement. Conversely, the combined channel/angle connections (Specimens R10-N8-G45-T and R6.3-N15-G50-T) exhibited lower ductility, failing at around 11 mm of vertical displacement. The improved ductility observed in blind-bolted connections results directly from the ductile behaviour of the Hollo-bolt due to the presence of a flexible sleeve. Conversely, it was concluded that for the combined channel/angle connections under shear loads, ductility was typically limited by brittle fracture of the bolts in shear rather than the failure of the other constituent components. In the case of combined channel/angle connections incorporating web angle components, the ductility was improved due to the increased number of standard bolts in shear. This connection configuration also exhibited higher shear resistance reaching the actuator force capacity at 9 mm without appreciable strength degradation.

A three-dimensional finite element model was developed to simulate the behaviour of bolted angle beam-to-tubular column connections under shear loading conditions. To assess the accuracy of the numerical model, results obtained by means of the FE models (including the initial stiffness, ultimate load and failure mode) were compared with the experimental response. Despite some differences, which are attributed to modelling idealisations and assumptions, the FE estimations were found to correlate well with experimental results in the small as well as large levels of displacement demands. This good agreement with the experimental results confirms that the detailed FE models are able to simulate the shear response of bolted angle connections with reasonable accuracy.

Finally, the applicability of component-based approaches for the estimation of connection design parameters was discussed. It was shown that such mechanical models can offer a reasonable estimation of connection stiffness and connection yield capacity. Similarly, it was shown that if the ultimate shear capacity is defined on the basis of the weakest components, reasonably conservative estimates are typically obtained.

Acknowledgements

The financial support of Tata steel Tubes for the research described in this paper is gratefully acknowledged. The authors would also like to thank the technical staff of the Structures Laboratories at Imperial College London, particularly Mr T. Stickland, for their assistance with the experimental work. Finally, the first author would like to acknowledge the support provided by China Scholarship Council and The UK Department for Innovation, Universities & Skills for the funding provided for her doctoral research studies through a UK/China Excellence Scholarship.

References

1. Cao J, Packer J, Kosteski N. Design guidelines for longitudinal plate to HSS connections. *Journal of Structural Engineering* 1998. 124(7): 784-791.
2. Kosteski N, Packer JA. Longitudinal plate and through plate-to-hollow structural section welded connections. *Journal of Structural Engineering* 2003. 129(4): 478-486.
3. Kosteski N, Packer JA. Welded tee-to-HSS connections. *Journal of Structural Engineering, ASCE* 2003. 129(2): 151-159.
4. Kurobane Y. Connections in tubular structures. In: *Progress in Structural Engineering and Materials*, 2002.
5. CEN.EN1993-1-8. Eurocode 3: Design of steel structures, Part 1-8: Design of joints. Vol. 1-8, 1998.
6. France JE, Buick Davison J, Kirby PA. Strength and rotational stiffness of simple connections to tubular columns using flowdrill connectors. *Journal of Constructional Steel Research* 1999. 50(1): 15-34.
7. Banks G. Flowdrilling for tubular structures, in *Proceedings of the Fifth International Symposium on Tubular Structures*, UK, 1993.
8. Korol R. Blind bolting W-shape beam to HSS columns. *Journal of Structural Engineering-ASCE* 1999. 119(12): 3463-3481.
9. Huck-International-Inc. Industrial fastening system. Arizona (USA), 1990.
10. Lindapter-International-Ltd. Type HB hollo-bolt for blind connection to structural steel and structural tubes. Lindapter International Ltd, UK, 1995.
11. Barnett T, Tizani W, Nethercot D. The practice of blind bolting connections to structural hollow sections: A review. *Steel and Composite Structures* 2001. 1(1): 1-16.
12. Barnett T, Tizani W, Nethercot D. Blind bolted moment resisting connections to structural hollow sections, in *Connections in Steel Structures IV*. Virginia, USA, 2000.
13. Elghazouli AY, Málaga-Chuquitaype C, Castro JM, Orton AH. Experimental monotonic and cyclic behaviour of blind-bolted angle connections. *Engineering Structures* 2009. 31(11): 2540-2553.
14. Yeomans NF. Rectangular hollow section column using Lindapter Hollobolt, in *Tubular Structures VIII*; Choo and van der Vegte (eds) Balkema: Rotterdam. 559-566, 1998.
15. De-Stefano M, De-Luca A, Astaneh-Asl A. Modeling of cyclic moment-rotationresponse of double-angle connections. *Journal of Structural Engineering* 1994. 120(1): 212-229.
16. Kishi N, Ahmed A, Yabuki N, Chen WF. Nonlinear finite element analysis of top and seat-angle with double web-angle connections. *Structural Engineering and Mechanics* 2001. 12(2): 201-214.
17. Kishi N, Chen WF. Moment-rotation relations of semi-rigid connections with angles. *Journal of Structural Engineering* 1990. 116(7): 1813-1834.
18. Ghobarah A, Mourad S, Korol RM. Moment-rotation relationship of blind bolted connections for HSS columns. *Journal of Constructional Steel Research* 1996. 40(1): 63-91.
19. Wang ZY, Tizani W, Wang QY. Strength and initial stiffness of a blind-bolt connection based on the T-stub model. *Engineering Structures* 2010. 32(9): 2505-2517.

20. Málaga-Chuquitaype C, Elghazouli AY. Component-based mechanical models for blind-bolted angle connections. *Engineering Structures* 2010. 32(10): 3048-3067.
21. Ding J, Wang YC. Experimental study of structural fire behaviour of steel beam to concrete filled tubular column assemblies with different types of joints. *Engineering Structures* 2007. 29(12): 3485-3502.
22. Málaga-Chuquitaype C, Elghazouli AY. Behaviour of combined channel/angle connections to tubular columns under monotonic and cyclic loading. *Engineering Structures* 2010. 32(6): 1600-1616.
23. Barnett T. The behaviour of a blind bolt for moment resisting connections in hollow steel sections. PhD thesis, School of Civil Engineering, University of Nottingham, 2001.
24. Liu Y. Behaviour of steel connections under extreme loading conditions. PhD Thesis, Department of Civil and Environmental Engineering, Imperial College London, UK, 2012.
25. ABAQUS. ABAQUS Theory Manual,Version 6.7. Hibbit, Karlsson and Sorensen Inc., 2003.
26. Vlassis AG, Izzuddin BA, Elghazouli AY, Nethercot DA. Progressive collapse of multi-storey buildings due to failed floor impact. *Engineering Structures* 2009. 31(7): 1522-1534.
27. Faella C, Piluso V, Rizzano G. Structural Steel Semi-Rigid Connections: Theory, Design and Software. Florida, USA: CRC Press, 2000.

Tables

Table 1: Summary of test programme for bolt shear characterization

Reference	Configuration Type	Bolt Type (G10.9 M16)	Bolt hole diameter (*mm*)	Connecting plate thickness(*mm*) (as shown in Figure 1)	
			d_0	d_1	d_2
S-10-8-H	A	Hollo-bolt	26	10	8
S-15-15-H	A	Hollo-bolt	26	15	15
D-8-10-H	B	Hollo-bolt	26	8	10
D-8-15-H	B	Hollo-bolt	26	8	15
S-10-8-N	A	Standard bolt	18	10	8
S-15-15-N	A	Standard bolt	18	15	15

Table 2: Material properties

Element	Yield stress (N/mm^2)	Ultimate stress (N/mm^2)
Beam UB 305×102×25	329	443
Column SHS 150×150×10	368	498
Column SHS 150×150×6.3	385	485
Column SHS 200×200×10	433	487
Angle L 100×75×8	312	438
Angle L 100×80×15	293	449
Hollo-bolt sleeve	382	512

Table 3: Summary of the test specimens

Reference	Type	Column	Angle	Reverse Channel cut from:	Dimensions (mm) (as shown in Figure 7)										
					a	b	c	d	e	f	g	h	i	k	l
H10-N8-G45-T	A	SHS 150×150×10	L100×75×8	-	45	30	35	65	-	-	-	100	45	-	-
H10-N8-G50-T	A	SHS 150×150×10	L100×75×8	-	50	50	35	40	-	-	-	100	45	-	-
H10-N15-G50-T	A	SHS 150×150×10	L100×80×15	-	50	100	35	45	-	-	-	100	45	-	-
R10-N8-G45-T	B	SHS 200×200×10	L100×75×8	SHS 150×150×10	45	30	35	65	-	-	-	100	45	515	70
R6.3-N15-G50-T	B	SHS 200×200×10	L100×80×15	SHS 150×150×6.3	50	100	35	45	-	-	-	100	45	465	70
R10-N8-G50-W	C	SHS 200×200×10	L100×75×8	SHS 150×150×10	50	50	45	30	40	90	15.5	-	-	465	70

Table 4: Summary of test results for bolted angle connections

Reference	Initial stiffness (kN/mm)	Shear force at yield (kN)	Shear force at 8mm displacement (kN)	Failure	
				Force (kN)	Displacement (mm)
H10-N8-G45-T	104	117	280	-	-
H10-N8-G50-T	91	95	303	-	-
H10-N15-G50-T	141	110	388	-	-
R10-N8-G45-T	98	128	283	322	11.2
R6.3-N15-G50-T	73	116	295	329	11.4
R10-N8-G50-W	288	205	584	-	-

Figures

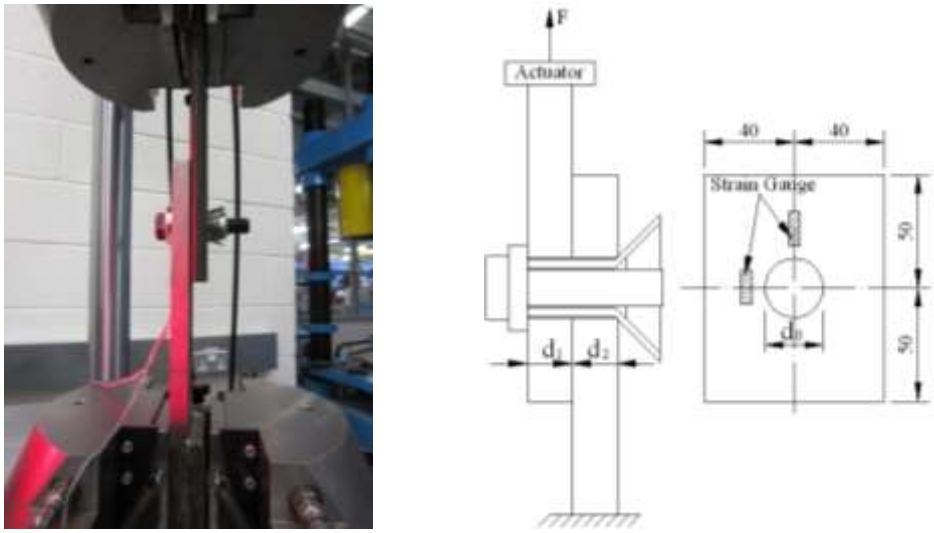

(a) Configuration Type A (simple shear): general view (left) and test arrangement (right).

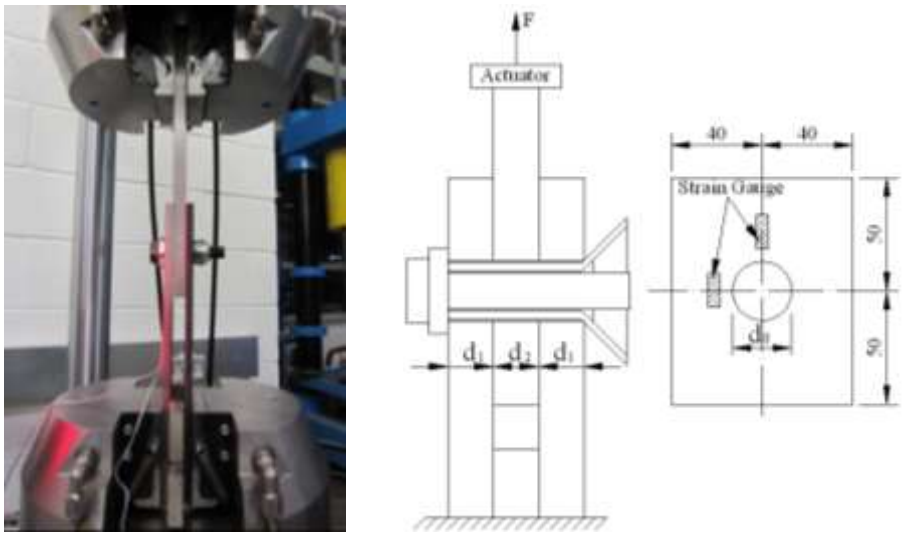

(b) Configuration Type B (double shear): general view (left) and test arrangement (right)

Figure 1: Test set-up for simple and double shear tests on bolts (dimensions in mm).

(a) S-10-8-H (b) S-15-15-H (c) D-8-10-H (d) D-8-15-H

Figure 2: Deformation modes of blind-bolts specimens in shear

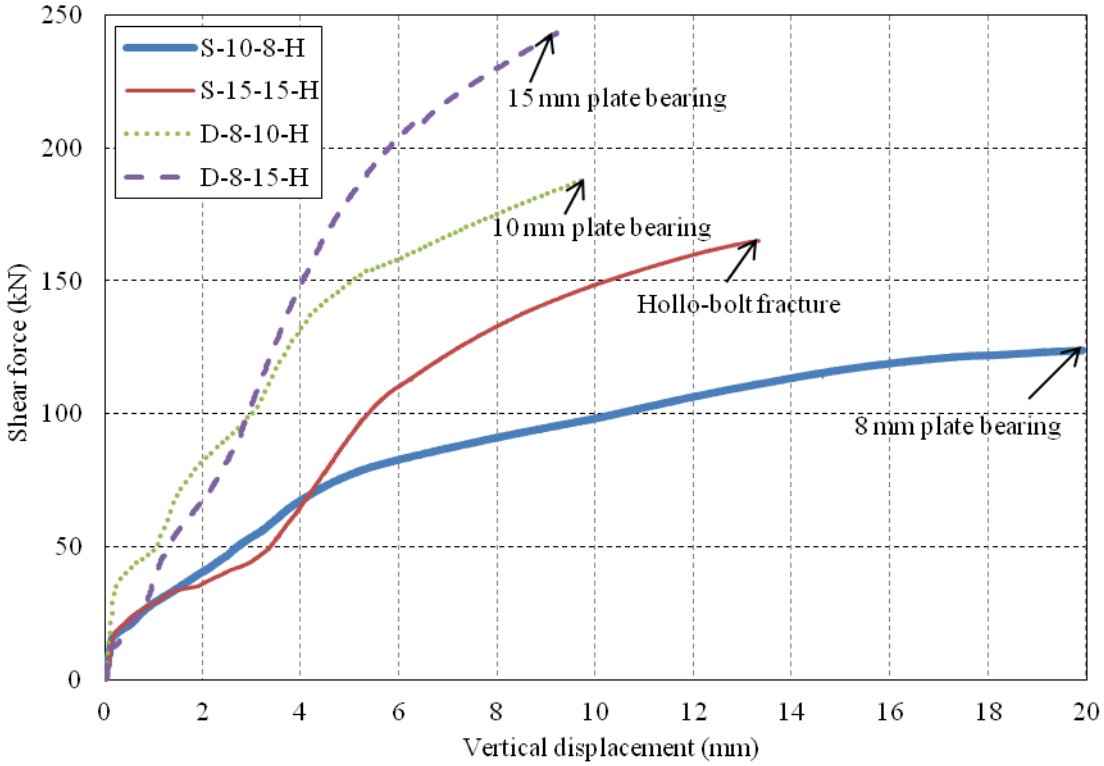

Figure 3: Shear force-displacement relationships for blind-bolts in tests

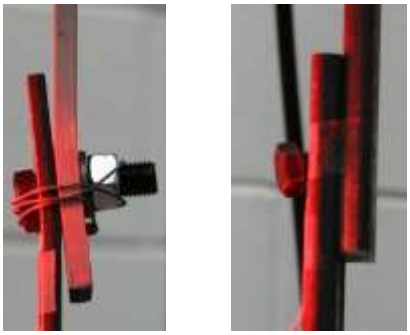

(a) S-10-8-N (b) S-15-15-N

Figure 4: Deformation mode of standard bolt in shear

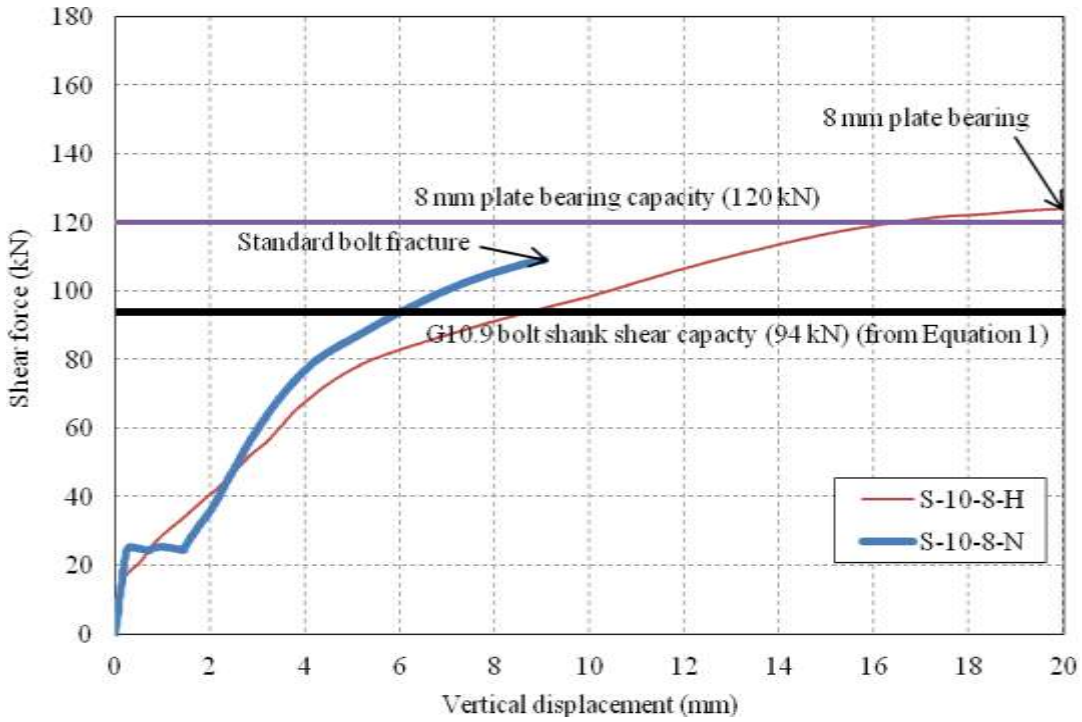

(a) Specimens S-10-8-H and S-10-8-N

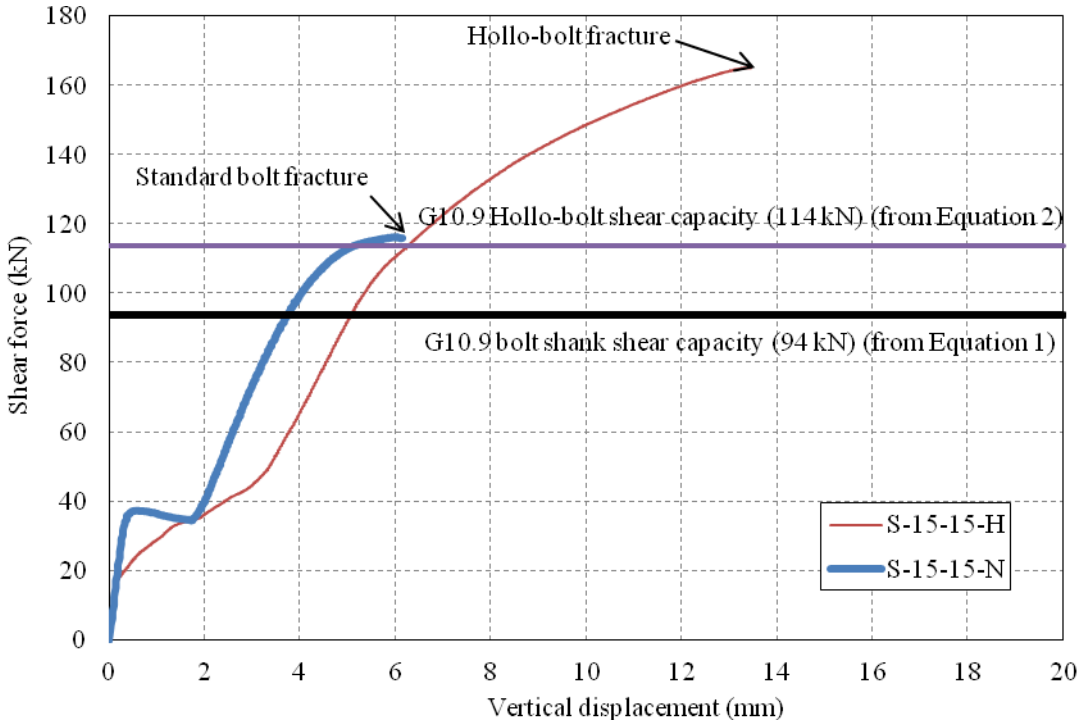

(b) Specimens S-10-15-H and S-15-15-N

Figure 5: Comparison of shear response between standard bolt and blind-bolt simple lap joint with different plate thicknesses

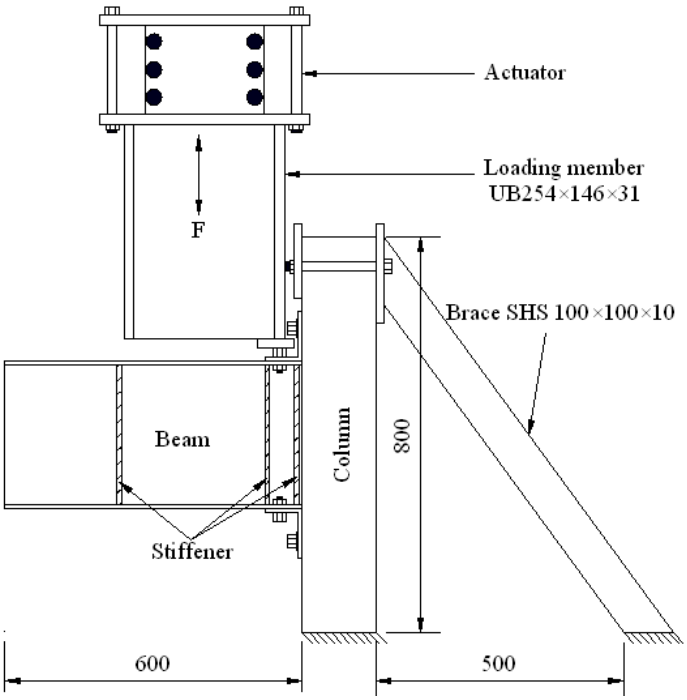

(a) Schematic representation of test set-up (dimensions in mm)

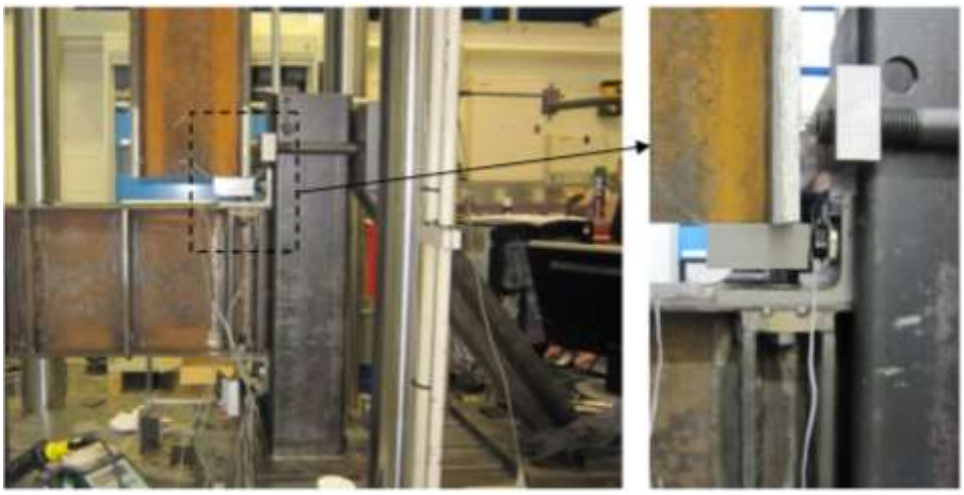

(b) General view of testing arrangement

Figure 6: Test set-up for bolted angle connections

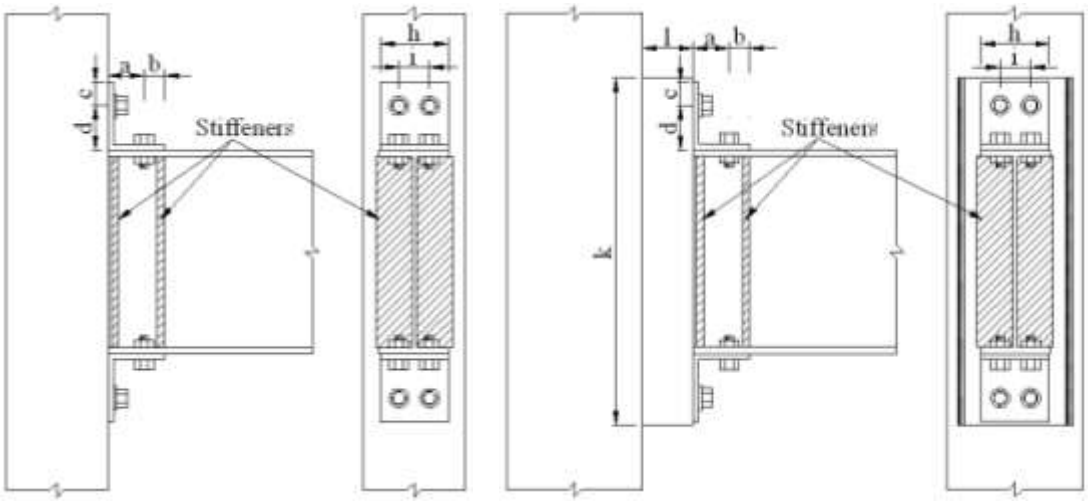

(a) Type A (b) Type B

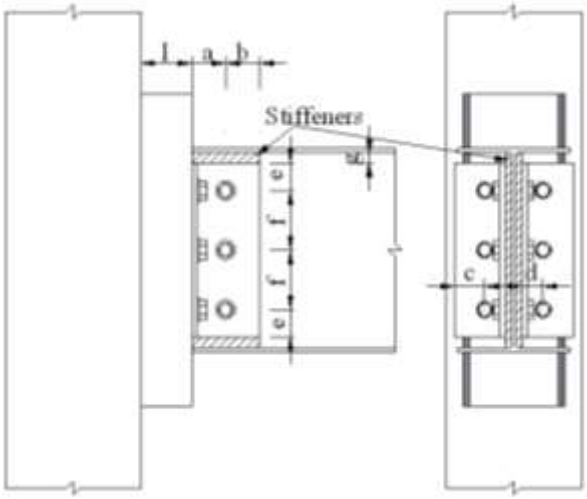

(c) Type C

Figure 7: Configuration of connection specimens

(a) Specimen H10-N8-G45-T (b) Specimen H10-N8-G50-T (c) Specimen H10-N15-G50-T

Figure 8: Main deformation patterns of blind-bolted angle connections at the end of the test

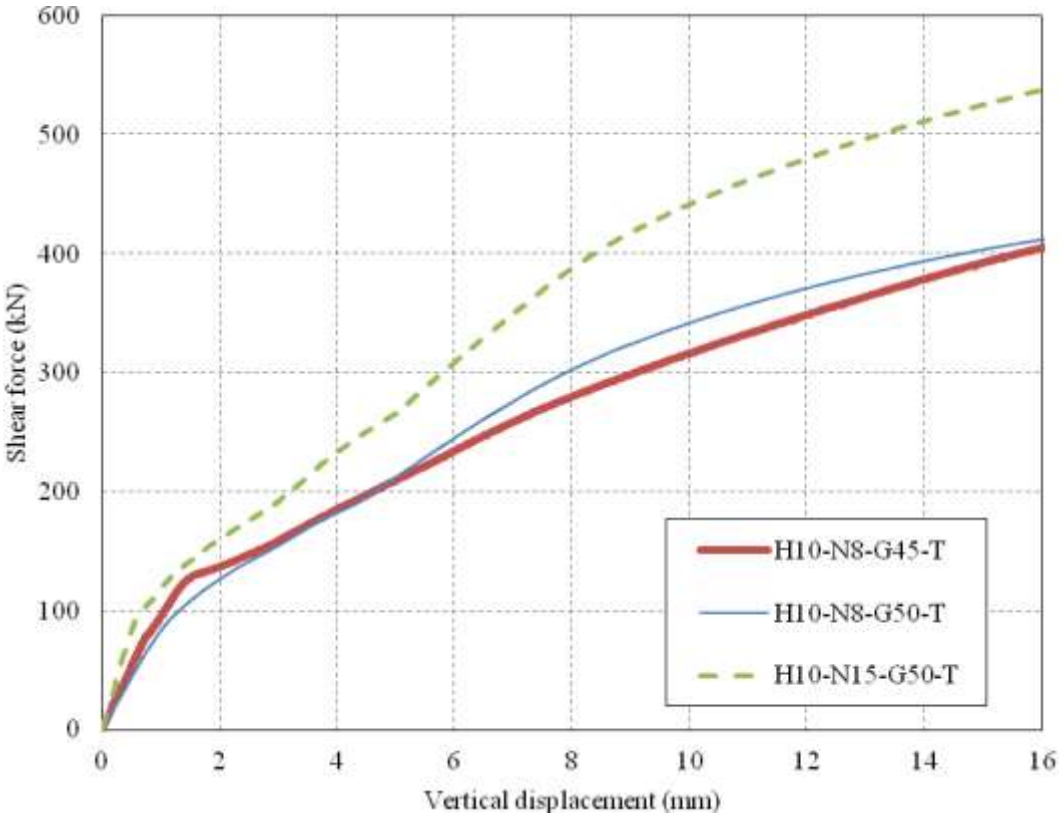

Figure 9: Shear force-displacement relationship for blind-bolted angle connections

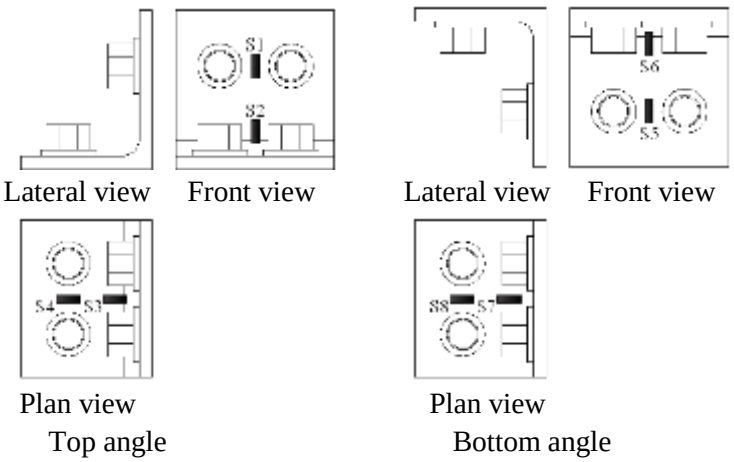

(a) Location of strain gauges blind-bolted connections

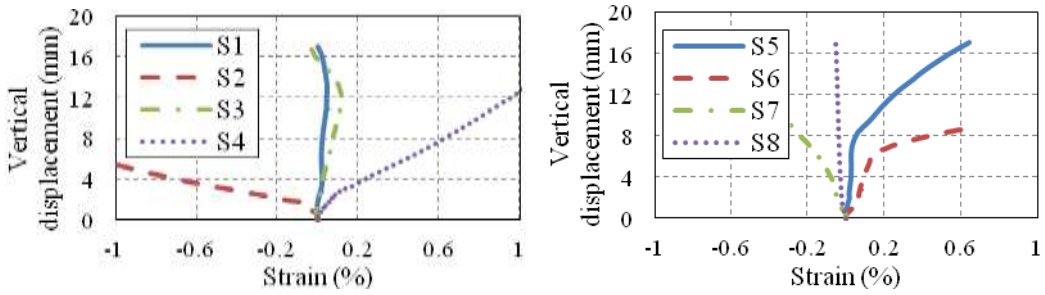

(b) Specimen H10-N8-G45-T

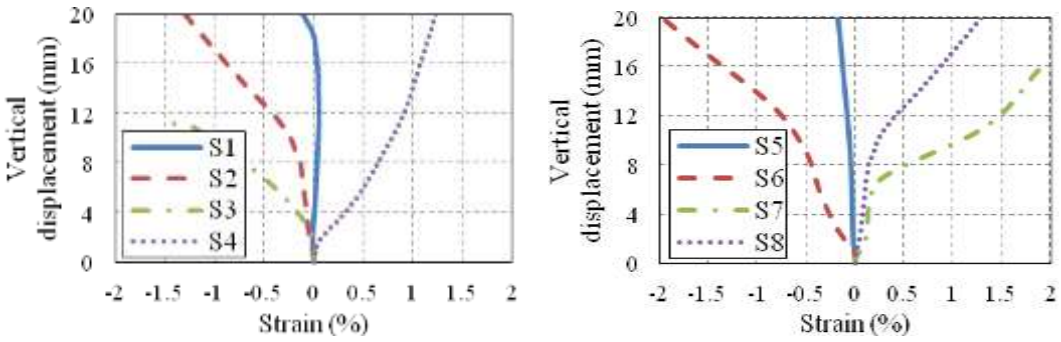

(c) Specimen H10-N8-G50-T

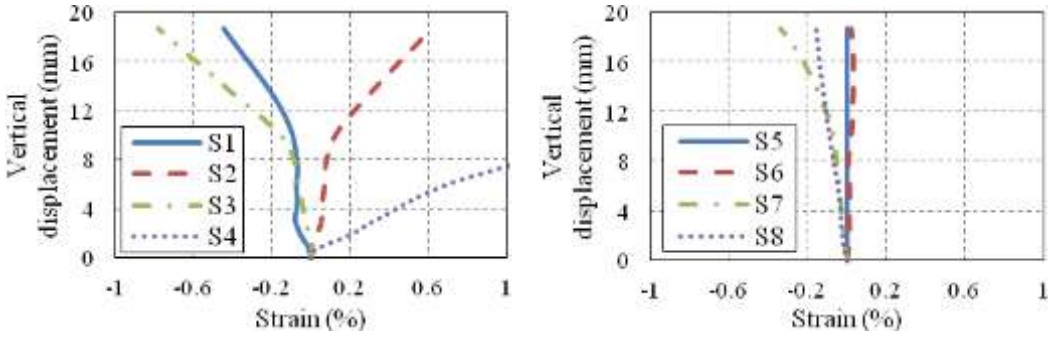

(d) Specimen H10-N15-G50-T

Figure 10: Measured strains in blind-bolted connections under shear

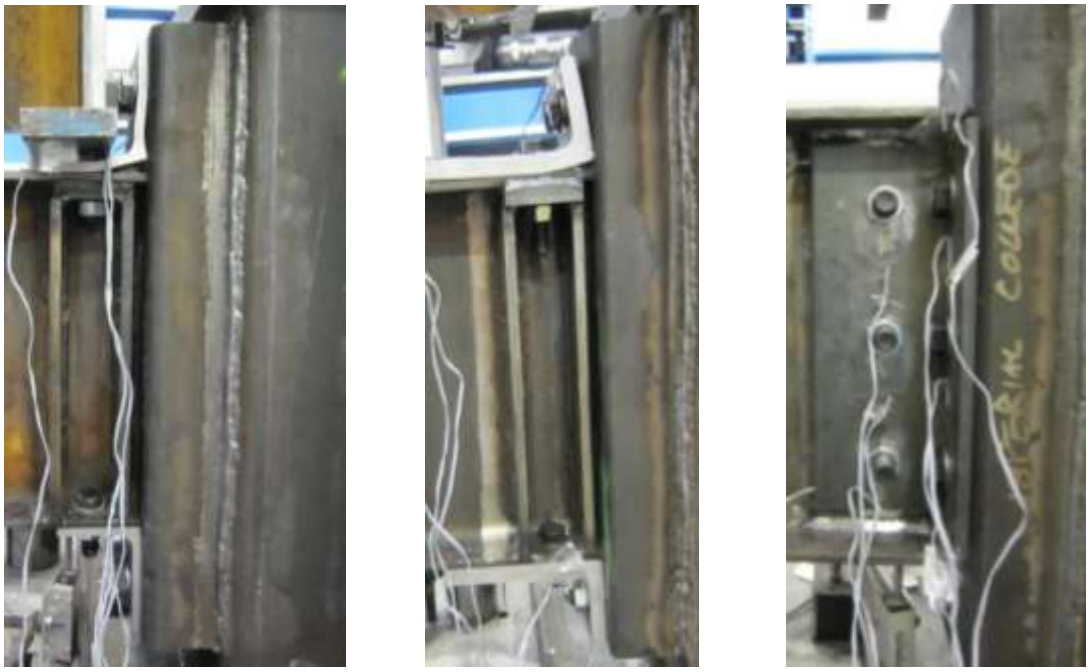

(a) Specimen R10-N8-G45-T (b) Specimen R6.3-N15-G50-T (c) Specimen R10-N8-G50-W

Figure 11: Deformation patterns of combined channel/angle connections at the end of test

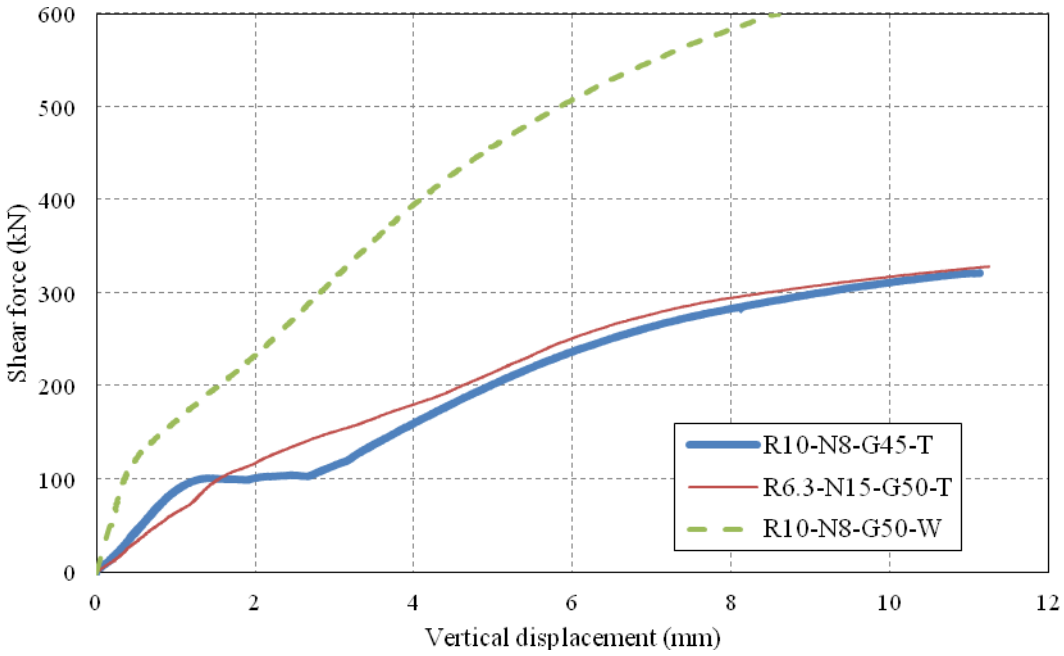

Figure 12: Experimental shear force-displacement relationship for combined channel/angle connections

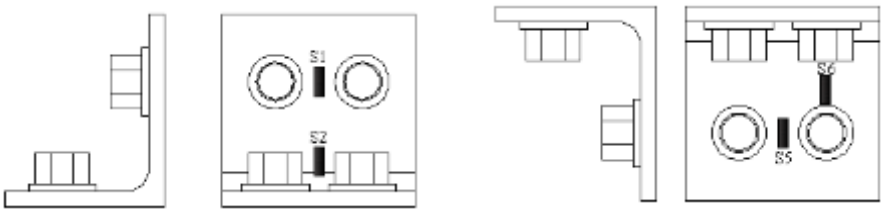

Lateral view Front view Lateral view Front view

Plan view Plan view

Top angle Bottom angle

(a) Location of strain gauges in top and seat reverse channel connections

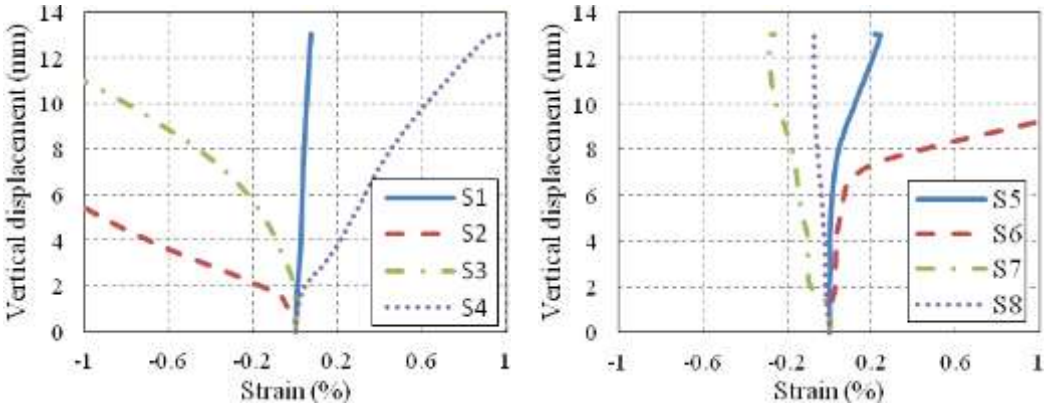

(b) Specimen R10-N8-G45-T

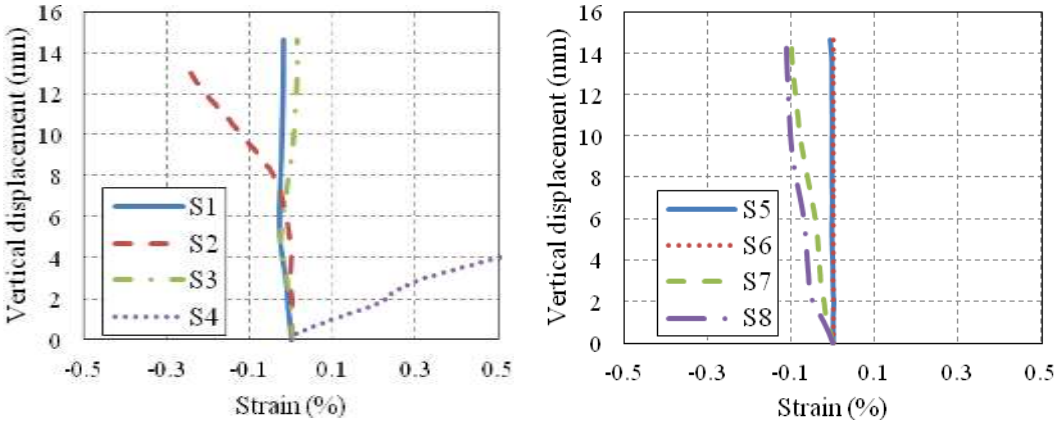

(c) Specimen R6.3-N15-G50-T

Figure 13: Measured strains for top and seat angle in reverse channel connections

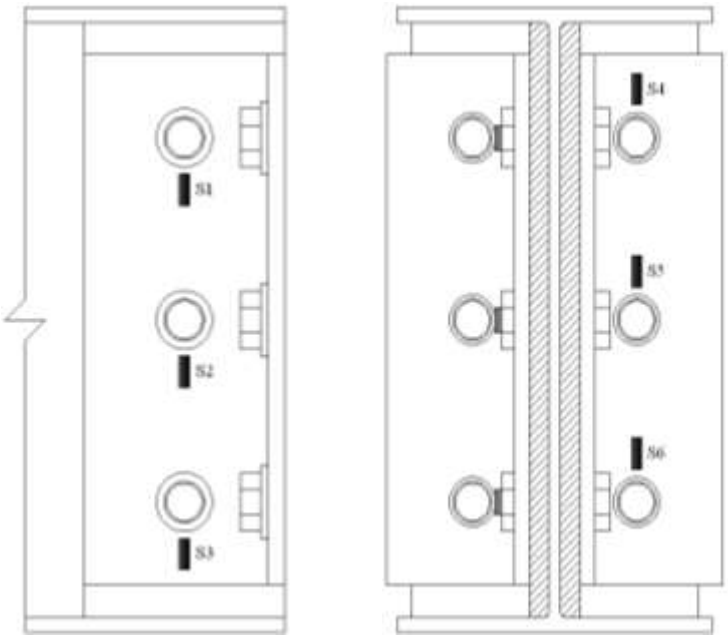

Lateral view Front view

(a) Location of strain gauges in web angle

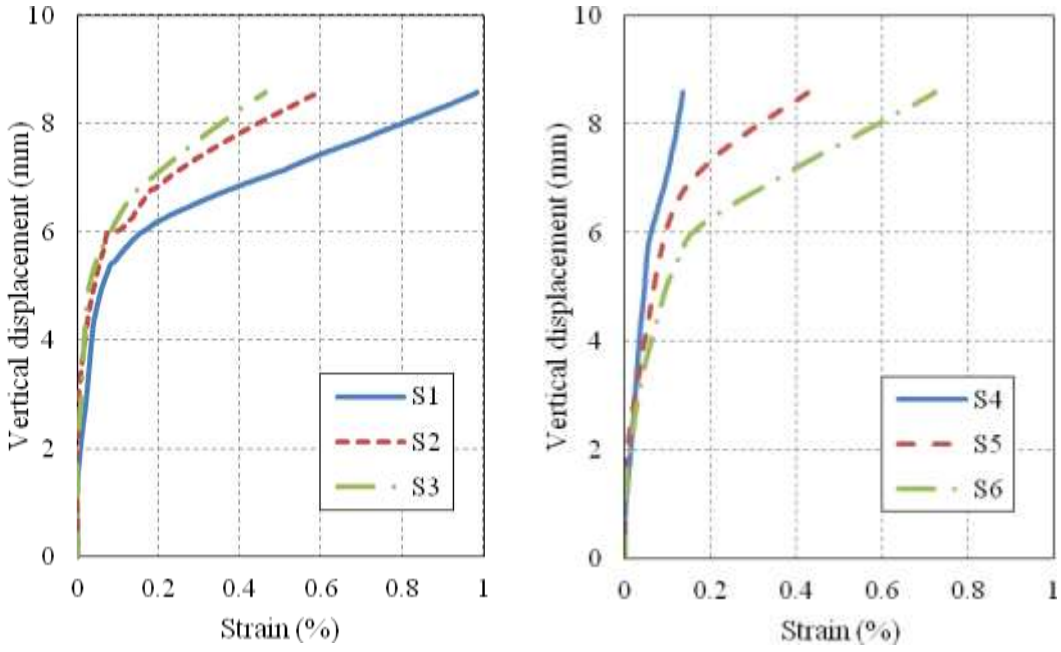

(b) Measured strains

Figure 14: Measured strains for web angle in Specimen R10-N8-G50-W

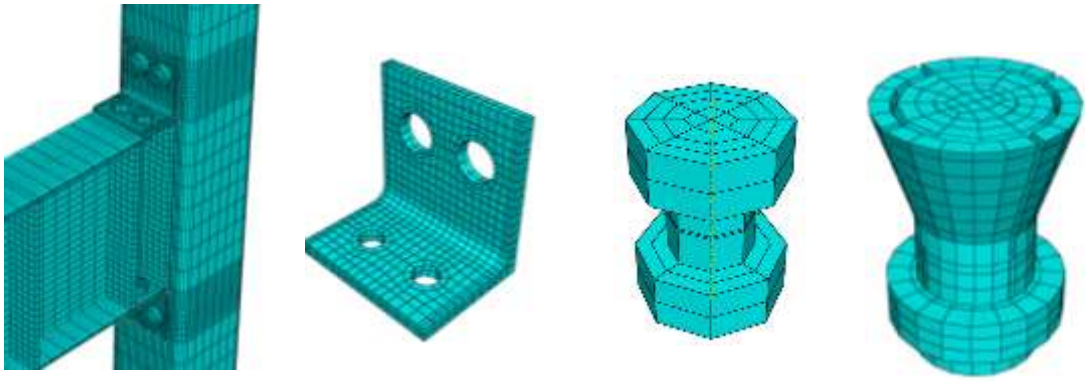

(a) Connection (b) Angle (c) Standard bolt (d) Hollo-bolt

Figure 15: FE representation of connection components

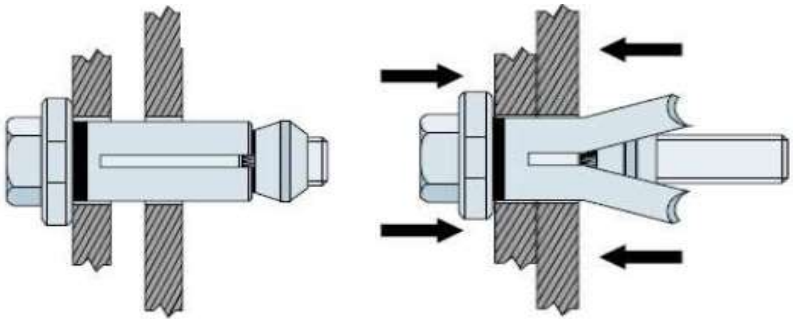

(a) Lindapter Hollo-bolt before (left) and after (right) installation

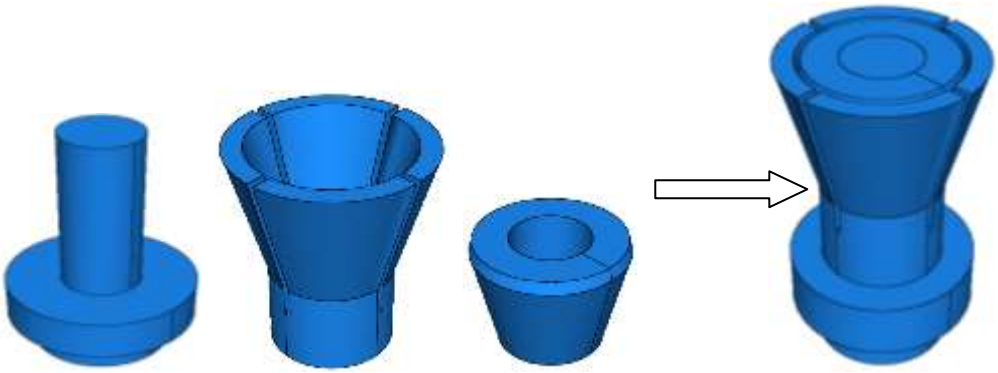

Central bolt Sleeve Cone Hollo-bolt

(b) Numerical model of Lindapter Hollo-bolt

Figure 16: Mechanism and FE modelling of Lindapter Hollo-bolt

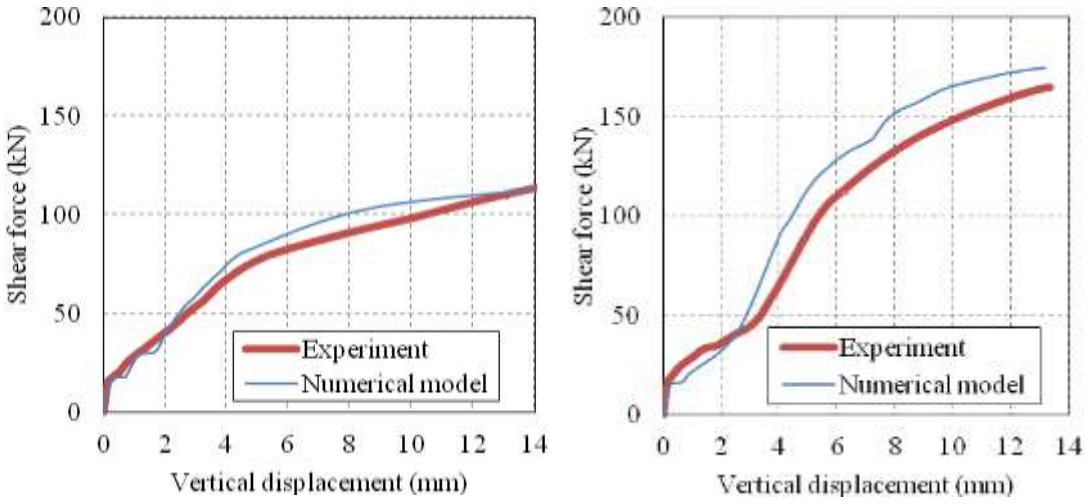

(a) S-10-8-H

(b) S-15-15-H

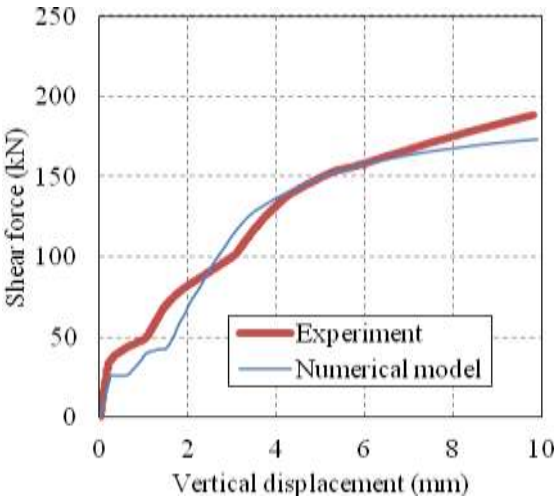

(c) D-8-10-H

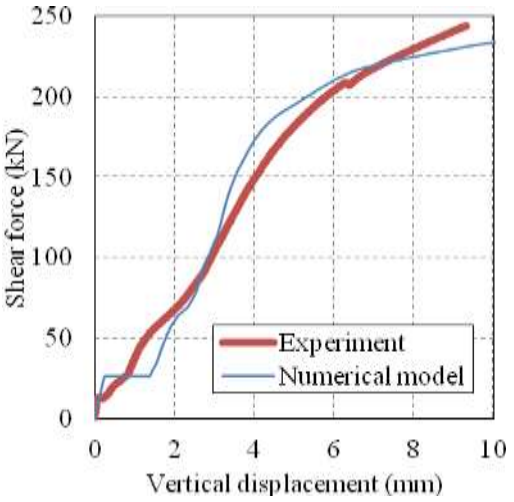

(d) D-8-15-H

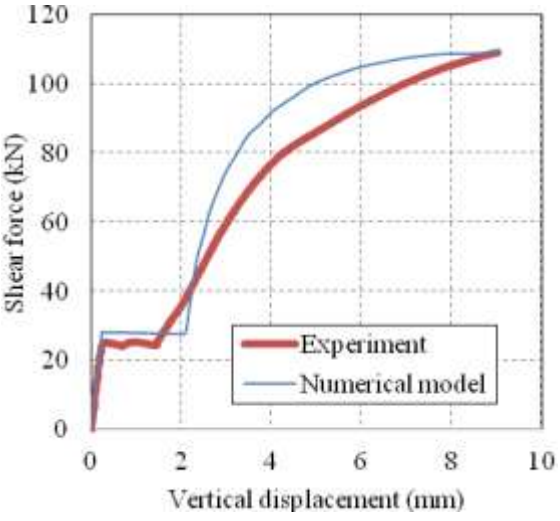

(e) S-10-8-N

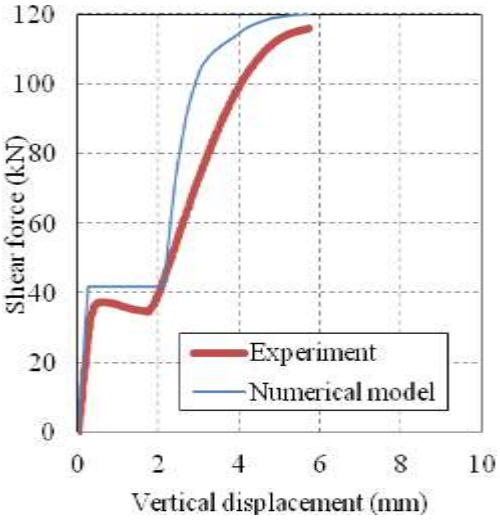

(f) S-15-15-N

Figure 17: Comparison of bolt shear force-displacement response between test and FE model

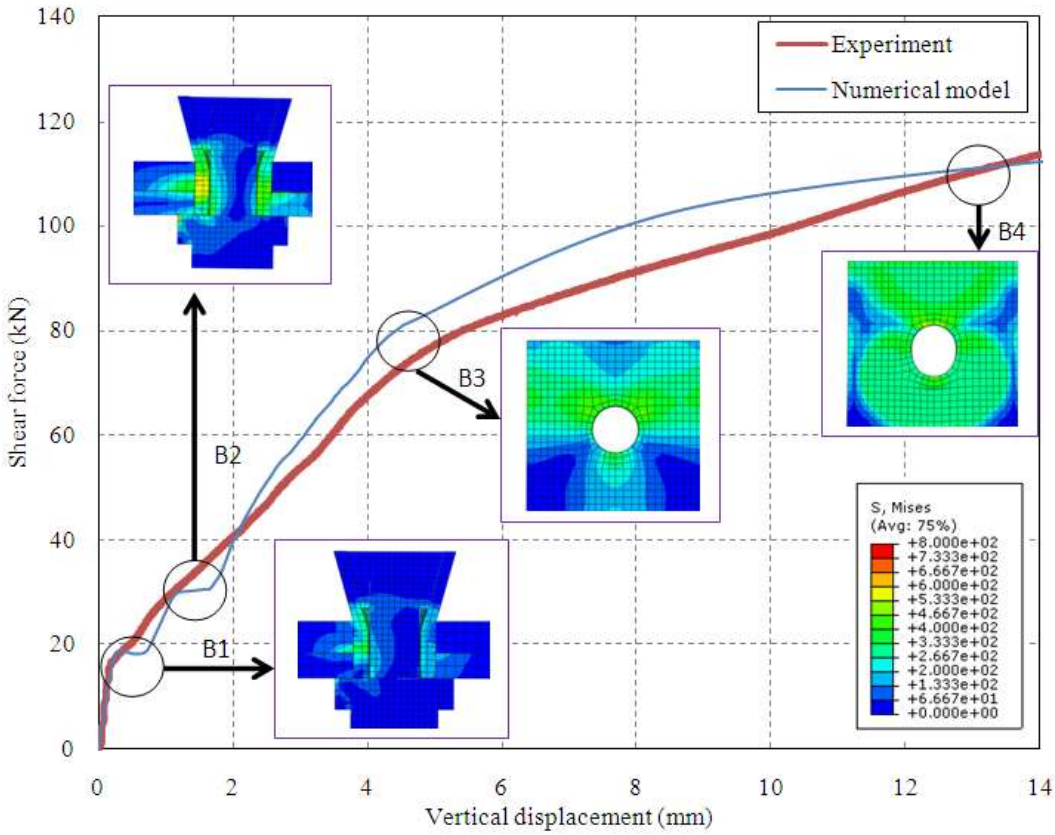

Figure 18: Comparison of shear behaviour for Specimen S-10-8-H between test and FE model

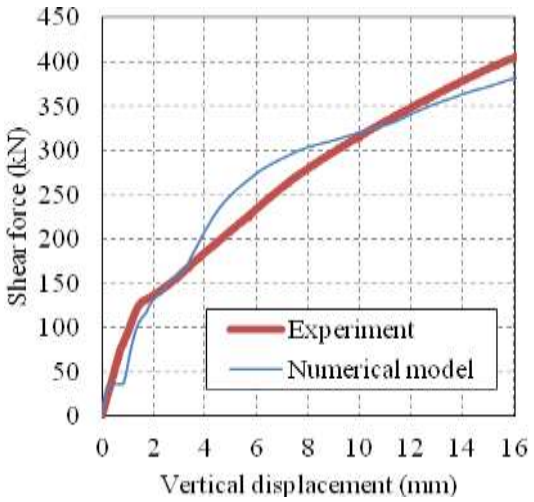

(a) Specimen H10-N8-G45-T

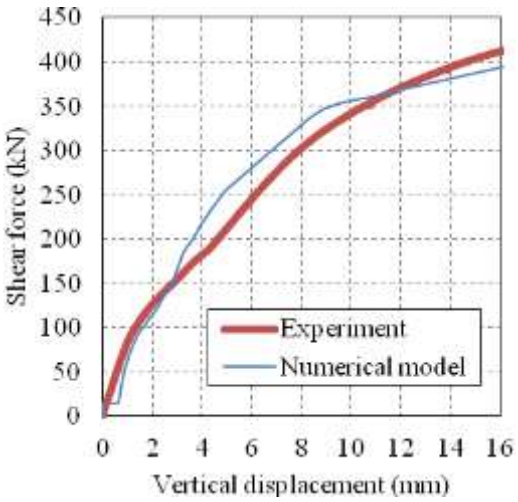

(b) Specimen H10-N8-G50-T

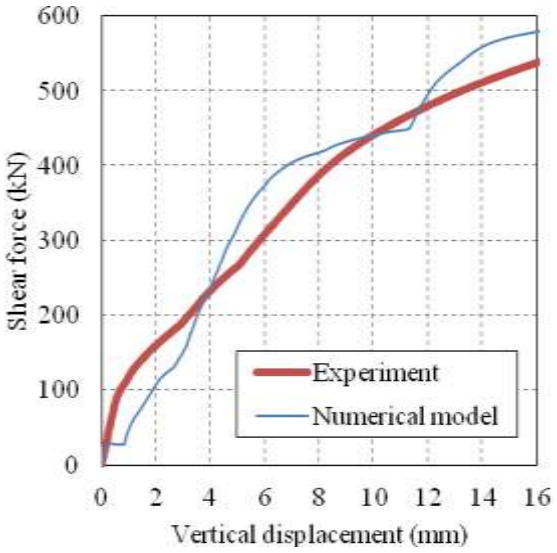

(c) Specimen H10-N15-G50-T

Figure 19: Comparison of experimental and numerical shear force-displacement response for blind-bolted angle connections

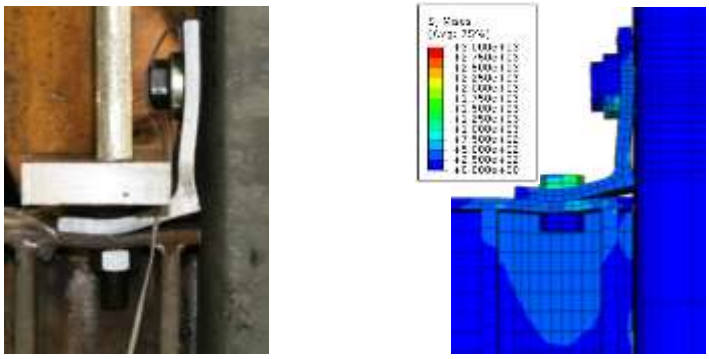

Experiment Numerical model

(a) Specimen H10-N8-G45-T

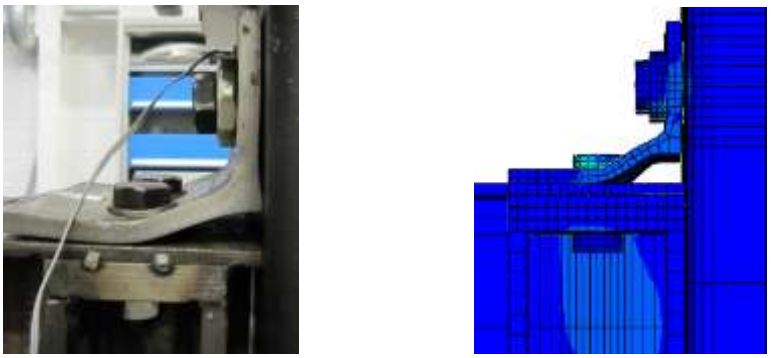

Experiment Numerical model

(b) Specimen H10-N8-G50-T

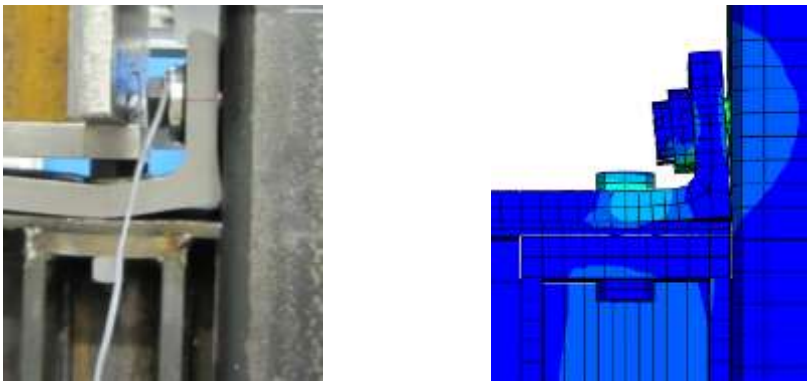

Experiment Numerical model

(c) Specimen H10-N15-G50-T

Figure 20: Comparison of top angle deformation patterns at a shear displacement of 16mm

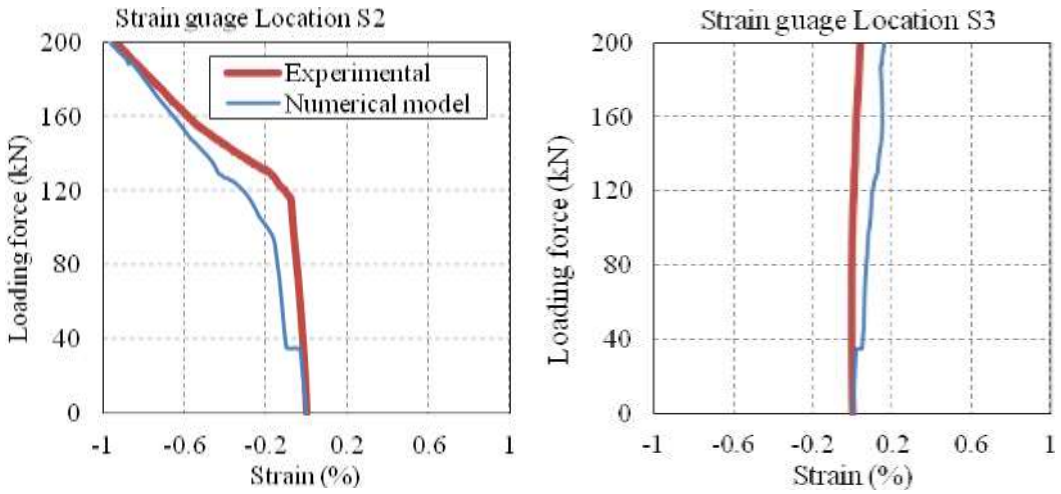

(a) Specimen H10-N8-G45-T

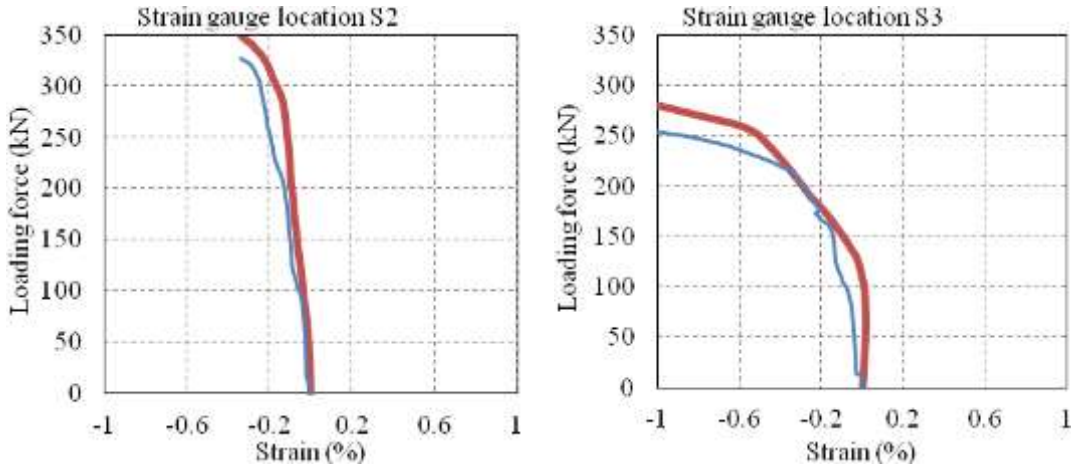

(b) Specimen H10-N8-G50-T

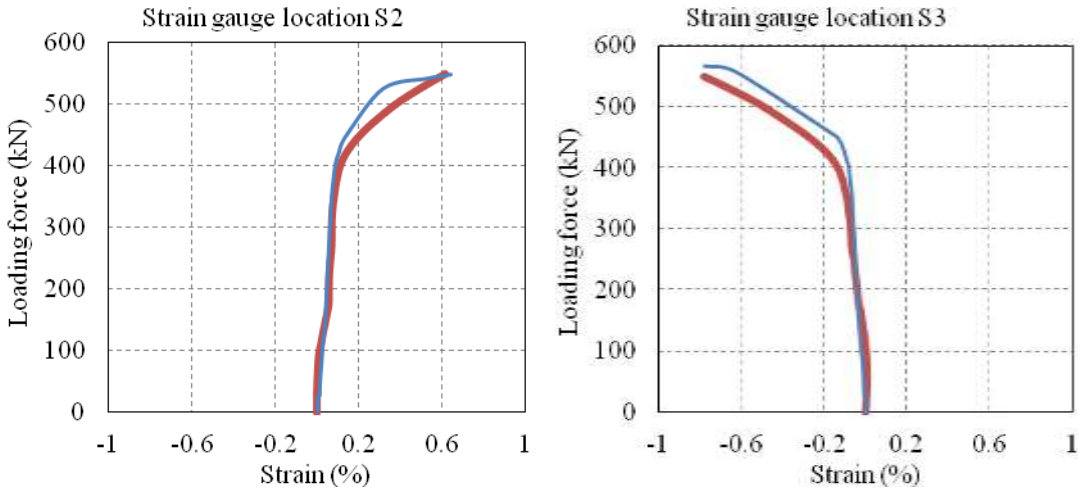

(c) Specimen H10-N15-G50-T

Figure 21: Comparison of strain value at Locations S2 and S3 (indicated in Figure 10) for blind-bolted angle connections

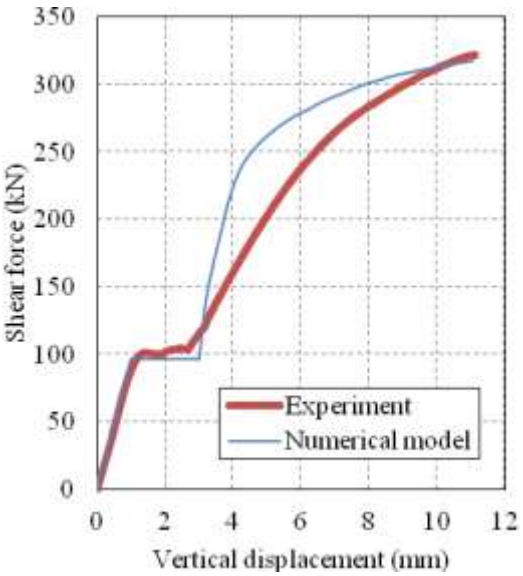

(a) Specimen R10-N8-G45-T

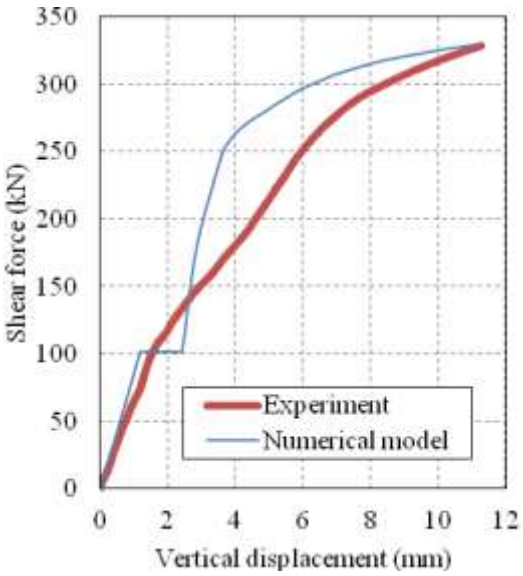

(b) Specimen R6.3-N15-G50-T

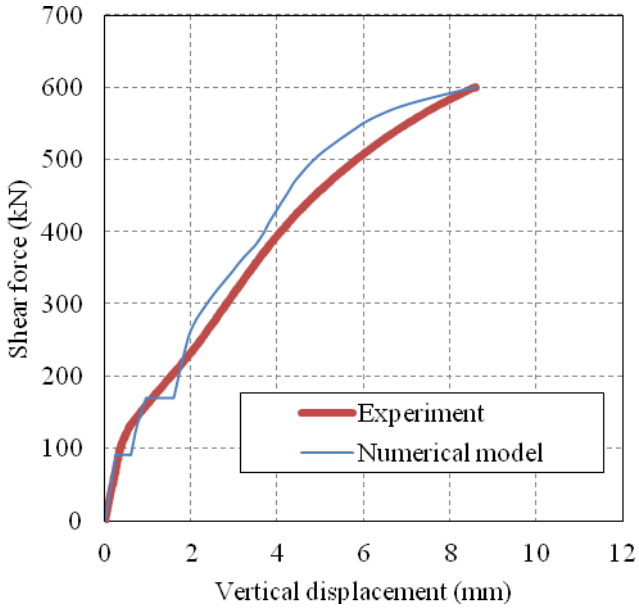

(c) Specimen R10-N8-G50-W

Figure 22: Comparison of experimental and numerical shear force-displacement response for combined channel/angle connections

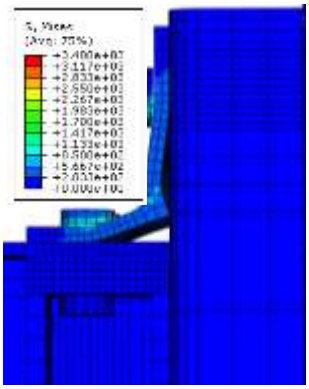

Experiment Numerical model

(a) Specimen R10-N8-G45-T

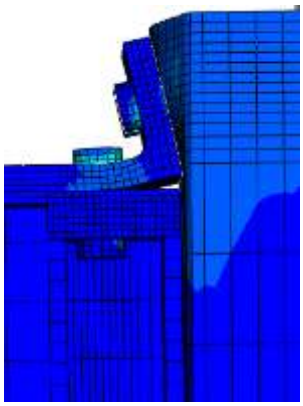

Experiment Numerical model

(b) Specimen R6.3-N15-G50-T

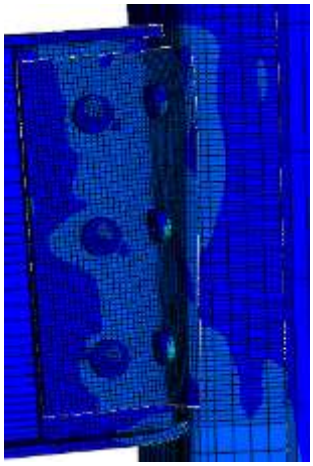

Experiment Numerical model

(c) Specimen R10-N8-G50-W

Figure 23: Comparison of top angle and web angle deformation patterns between the experiment and FE model at the end of the tests

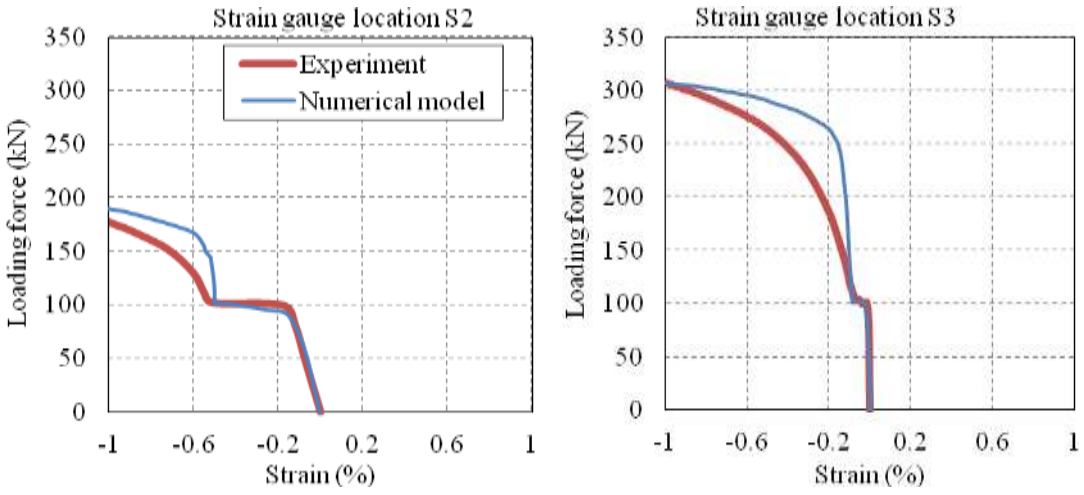

(a) Specimen R10-N8-G45-T

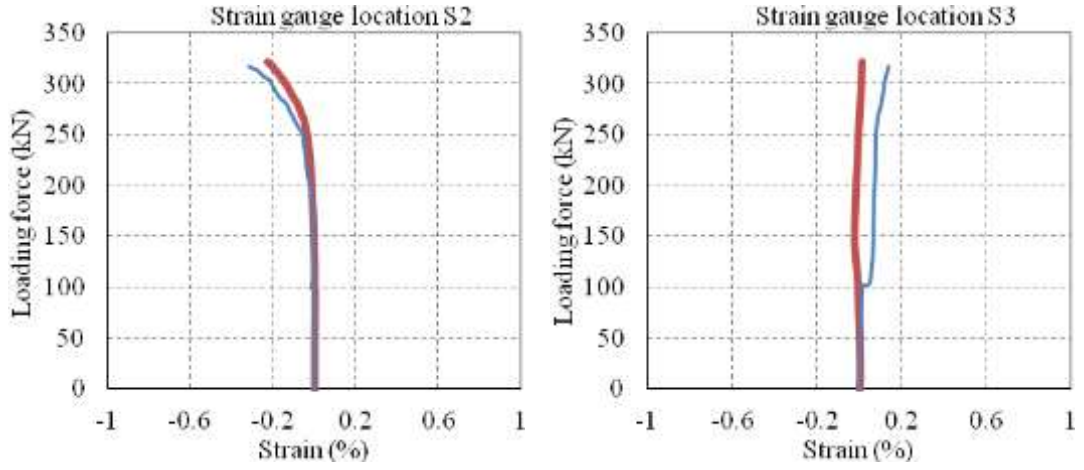

(b) Specimen R6.3-N15-G50-T

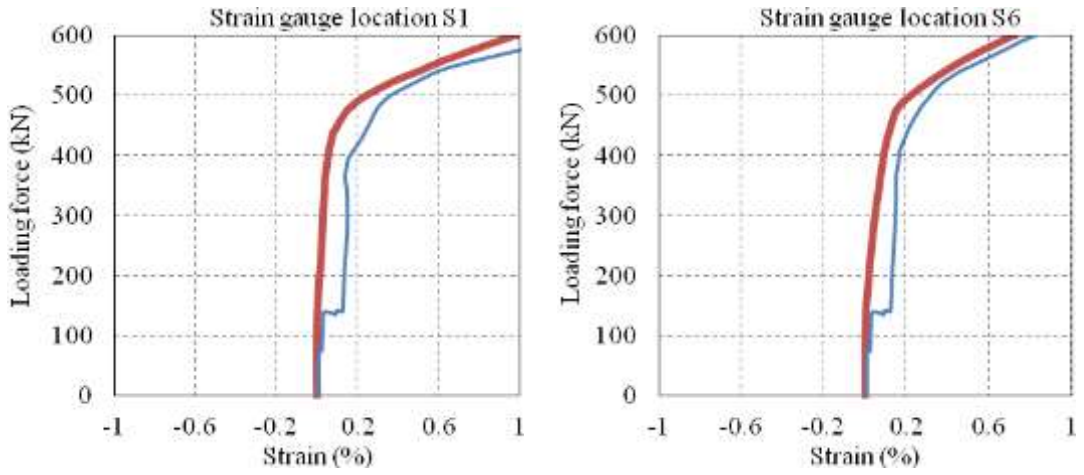

(c) Specimen R10-N8-G50-W

Figure 24: Comparison of strain value at Locations S2 and S3 (indicated in Figure 13) for combined channel/angle connections as well as Locations S1 and S6 (indicated in Figure 14) for web angle connections

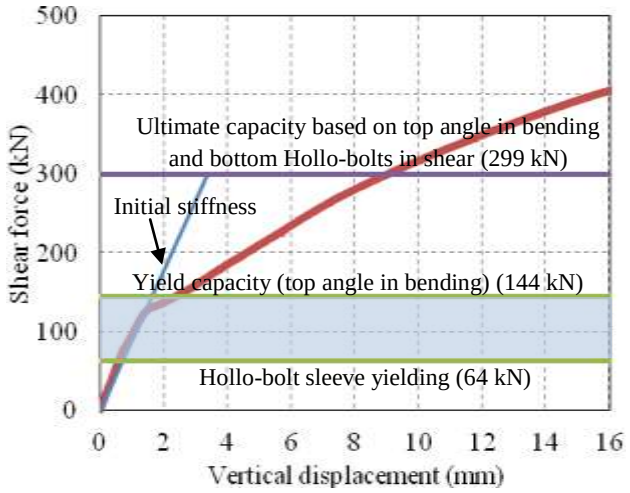

(a) Specimen H10-N8-G45-T

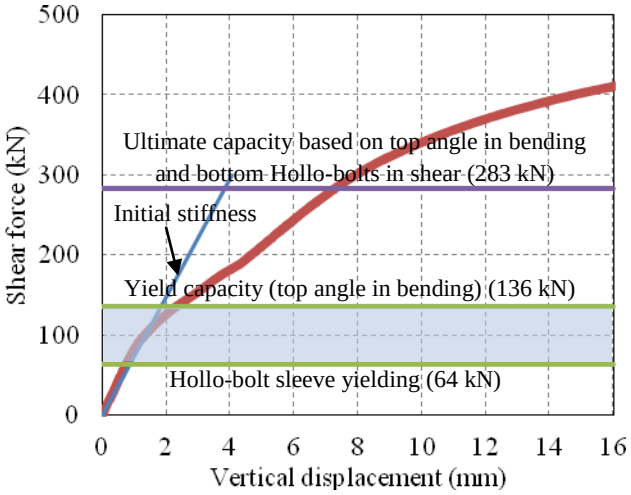

(b) Specimen H10-N8-G50-T

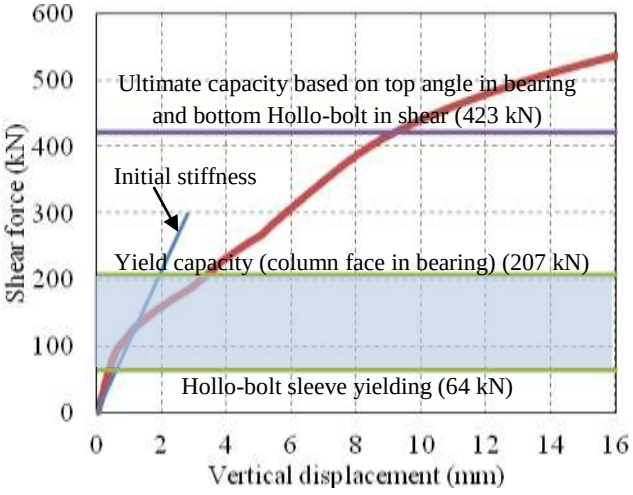

(c) Specimen H10-N15-G50-T

Figure 24: Comparison of experimental response and component-based estimations for Hollo-bolted angle connections

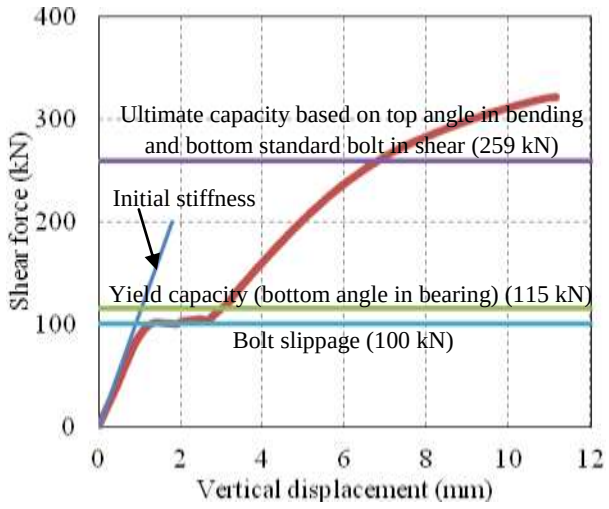

(a) Specimen R10-N8-G45-T

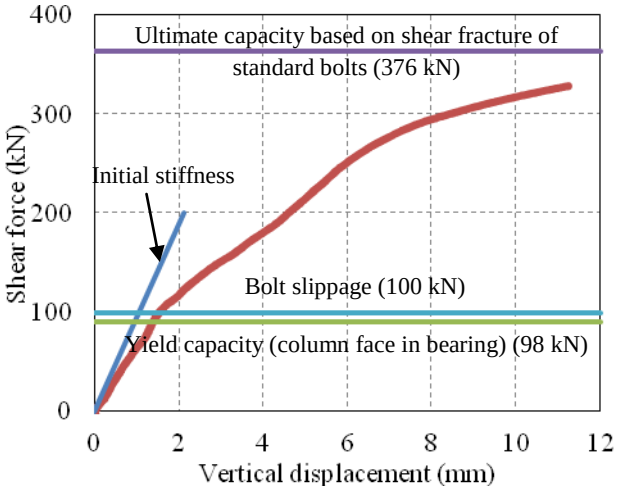

(b) Specimen R6.3-N15-G50-T

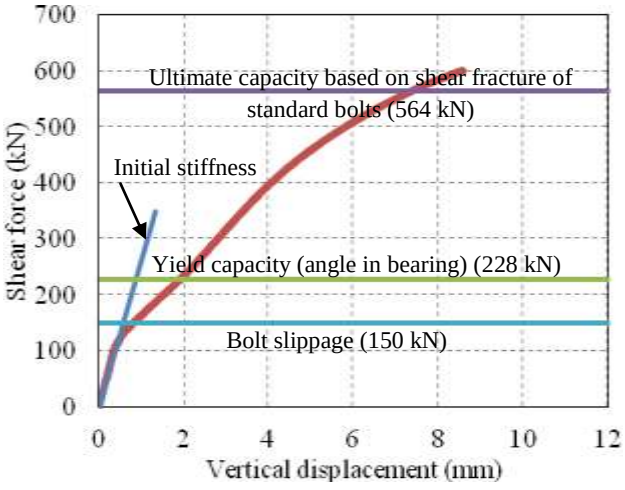

(c) Specimen R10-N8-G50-W

Figure 25: Comparison of experimental response and component-based estimations for combined channel/angle connections